Numerical simulations of tidal and wind-driven circulation in the Cretaceous Interior Seaway of North America

MARC C. ERICKSEN
RUDY SLINGERLAND } *Department of Geosciences, The Pennsylvania State University, University Park, Pennsylvania 16802*

ABSTRACT

Twenty-two numerical experiments using a multi-layer, numerical model of turbulent flow in shallow seas better define fluid circulation and sediment transport paths in the Cretaceous Interior Seaway of North America. Each experiment consists of a different combination of paleogeography, paleobathymetry, Coriolis acceleration, boundary tidal amplitudes, wind stresses, and bed friction. The paleogeographies and paleobathymetries represent three seaway configurations: a seaway of intermediate size and depth (200 m) during a transgressive peak (T5) in late Albian time; a seaway of maximum size and depth (400 m) during peak transgression (T6) in early Turonian time; and a seaway of minimum size and depth (100 m) during a peak regression (R8) in the Campanian. Values for the other key model parameters are: M_2 co-oscillating boundary tides of 0.1 to 0.2 m range at the Arctic Ocean boundary and 0.5 to 1 m range at the proto–Gulf of Mexico boundary; Coriolis accelerations corresponding to 30°N, 45°N, and 60°N latitude; Chezy friction factors ranging from 31 to 70 $m^{1/2} s^{-1}$; and average winter winds and two winter storms computed by the community climate model at the National Center for Atmospheric Research for paleogeographic conditions during the late Albian. Results of the numerical experiments, and comparison of these results with geologic observations, allow the following conclusions. (1) Circulation in the seaway was generally storm-dominated. (2) Typical winter storms crossing the seaway from west to east generated 0.3 $m\ s^{-1}$ shore-parallel, geostrophic currents on the shelves north of Arizona, at first flowing weakly to the north, but later during the storm, flowing strongly to the south. (3) Extreme storms could have produced 0.8 $m\ s^{-1}$ currents over the shelves, and 0.3 $m\ s^{-1}$ currents in 200 m of water. (4) Co-oscillating tides propagated into the seaway as progressive Kelvin waves, and therefore tidal ranges in the seaway were mesotidal to macrotidal along the southeastern margin but microtidal everywhere else. (5) Significant deep-water wave heights and periods of the fully developed wave field are predicted to have been 5 to 6 m high and 10 s, respectively. The northwestern shore of the seaway would have experienced these storm waves approaching from the north, and thus net sediment drift should have been to the south. Limited available field data support these conclusions.

INTRODUCTION

The Cretaceous Interior Seaway of North America was a large, epicontinental sea which flooded a foreland basin east of the Cordilleran thrust belt. From late Albian time through the remainder of the Cretaceous, the seaway connected the proto–Gulf of Mexico with the Cretaceous Arctic Ocean, attaining a maximum width of more than 1,000 km. Fluctuations in eustatic, tectonic, and climatic conditions of the seaway caused key oceanographic parameters (paleogeography, paleobathymetry, stratification, wind stresses, and boundary tides) to vary widely throughout the seaway's history. These fluctuations, in turn, must have caused variations in its circulation and sediment-transport regimes, but these are very poorly known. In the absence of modern analogues, geologists have used a number of approaches to determine the circulation of the seaway, including oxygen- and carbon-isotope studies to infer density stratification and resulting circulation (Wright, 1987), numerical modeling of tidal circulation (Slater, 1985), qualitative predictions of current patterns from inferred climatic conditions (Parrish and Curtis, 1982; Lloyd, 1982), characterizations of the paleoceanography from the distribution of paleobiogeographic units (Kauffman, 1984), numerical modeling of wind-driven flows over a portion of the Campanian shelf (Parrish and others, 1984), and empirical modeling derived from the distributions of lithofacies and measurement of paleocurrent indicators. Although these have been helpful, the qualitative studies often failed to consider physical controls exerted by the key oceanographic parameters, and the more physically based studies, such as those by Slater (1985) and Parrish and others (1984), treated only certain aspects of the circulation. Disagreements still persist, for example, on the influence of tides in the basin. Klein and Ryer (1978) concluded that the Cretaceous Interior Seaway had normal astronomical tides, and Ryer and Kauffman (1980) postulated that tidal range increased northward in the seaway along the western shoreline, reaching mesotidal levels as far north as southern Alberta. On the other hand, Leckie and Walker (1982) and Slater (1985) suggested that the seaway was generally microtidal. There are also differing opinions on what processes generated the shelf sand ridges in the seaway. A minority maintains that tides may have been important (for example, Leckie, 1986), whereas most believe that the ridges were emplaced by storm-generated currents (for example, Spearing, 1976; Boyles and Scott, 1982b; Swift and Rice, 1984; Swift and others, 1987).

Numerical modeling is an effective means of shedding light on the tidal and wind-driven circulation of this seaway, and epeiric seas in general. Two major achievements in the past decade make such modeling feasible and timely. First, hydrodynamic models have been developed and calibrated that are capable of accurately simulating the three-dimensional circulation of complex, nonhomogeneous bodies of water driven by both tides and winds (Leendertse and Liu, 1977, 1979; Nihoul, 1982; Heaps, 1987). Slater (1985), Slingerland (1986), and Ericksen and others (1989) presented initial studies applying such models to ancient systems. Second, atmospheric general-circulation models have developed to the stage where they can be applied to study atmospheric circulation for different paleogeographies (Barron, 1985). Indeed, Barron and co-workers (1982, 1984, 1985) have completed several climatic experiments for the Cretaceous, and their results indicate that paleo-

Geological Society of America Bulletin, v. 102, p. 1499–1516, 14 figs., 5 tables, November 1990.

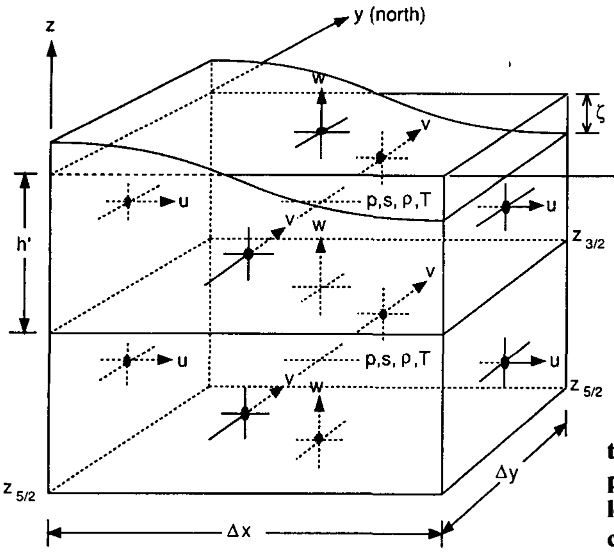

Figure 1. The layered structure of the model and relative position of variables. Fluid velocities are calculated at face-centered positions; the other dependent variables are calculated at cell centers (from Leendertse and others, 1973).

TABLE 2. VARIABLE DEFINITIONS AND UNITS IN THE MODEL

x, y, z	= Cartesian coordinates, positive eastward, northward, and upward (cm)
u, v, w	= respective components of velocity (cm/s)
t	= time (s)
f	= Coriolis parameter (s^{-1})
p	= pressure (dynes/cm^2)
s	= salinity (g/kg)
T	= temperature (°C)
ρ, ρ_a	= density of water (g/cm^3), air (1.226×10^{-3} g/cm^3)
$\bar{\rho}$	= reference density, a constant (g/cm^3)
ρ'	= departure from $\bar{\rho}$ depending on salinity and temperature
κ	= vertical mass diffusion coefficient
κ'	= vertical thermal diffusion coefficient
τxx, τxy, τyx, τyy, τxz, τyz	= components of the stress tensor (dynes/cm^2)
D_x, D_y	= horizontal diffusion coefficients
τ^s_x, τ^s_y	= wind stress (dynes/cm^2)
τ^b_x, τ^b_y	= bed stress (dynes/cm^2)
w_a	= wind speed (cm/s)
Ψ	= angle between wind direction and y axis (degrees)
C*	= wind drag coefficient
C	= Chezy coefficient ($cm^{1/2}s^{-1}$)

TABLE 1. HYDRODYNAMIC EQUATIONS FOR CIRCULATION IN EPEIRIC SEAS

Dynamic equations for circulation and sediment transport		
X-DIR equation of motion	$\frac{\partial u}{\partial t}+\frac{\partial(uu)}{\partial x}+\frac{\partial(uv)}{\partial y}+\frac{\partial(uw)}{\partial z}-fv+\frac{1}{\rho}\frac{\partial p}{\partial x}-\frac{1}{\rho}\left(\frac{\partial\tau_{xx}}{\partial x}+\frac{\partial\tau_{xy}}{\partial y}+\frac{\partial\tau_{xz}}{\partial z}\right)=0$	
Y-DIR equation of motion	$\frac{\partial v}{\partial t}+\frac{\partial(uv)}{\partial x}+\frac{\partial(vv)}{\partial y}+\frac{\partial(vw)}{\partial z}-fu+\frac{1}{\rho}\frac{\partial p}{\partial y}-\frac{1}{\rho}\left(\frac{\partial\tau_{yx}}{\partial x}+\frac{\partial\tau_{yy}}{\partial y}+\frac{\partial\tau_{yz}}{\partial z}\right)=0$	
Z-DIR equation of motion	$\frac{\partial p}{\partial z}+\rho g=0$	
Continuity of fluid	$\frac{\partial u}{\partial x}+\frac{\partial v}{\partial y}+\frac{\partial w}{\partial z}=0$	
Continuity of salt	$\frac{\partial s}{\partial t}+\frac{\partial(us)}{\partial x}+\frac{\partial(vs)}{\partial y}+\frac{\partial(ws)}{\partial z}-\frac{\partial\left(D_x\frac{\partial s}{\partial x}\right)}{\partial x}-\frac{\partial\left(D_y\frac{\partial s}{\partial y}\right)}{\partial y}-\frac{\partial\left(\kappa\frac{\partial s}{\partial z}\right)}{\partial z}=0$	
Continuity of heat	$\frac{\partial T}{\partial t}+\frac{\partial(uT)}{\partial x}+\frac{\partial(vT)}{\partial y}+\frac{\partial(wT)}{\partial z}-\frac{\partial\left(D_x\frac{\partial T}{\partial x}\right)}{\partial x}-\frac{\partial\left(D_y\frac{\partial T}{\partial y}\right)}{\partial y}-\frac{\partial\left(\kappa'\frac{\partial T}{\partial z}\right)}{\partial z}=0$	
Equation of state	$\rho=\bar{\rho}+\rho'(s,T)$	
Boundary conditions		
Wind stress	$\tau^s_x=C^*\rho_a w_a^2\sin\Psi$	$\tau^s_y=C^*\rho_a w_a^2\cos\Psi$
Bed stress	$\tau^b_y=\rho g\frac{v\sqrt{u^2+v^2}}{C^2}$	$\tau^b_x=\rho g\frac{u\sqrt{u^2+v^2}}{C^2}$
Open boundary		Tide or current

geography and topography are important factors governing the character of atmospheric circulation and, thus, ocean circulation. These Cretaceous climate experiments provide a unique opportunity to simulate circulation in the Cretaceous Interior Seaway with an atmospheric forcing consistent with Cretaceous paleogeography. The purpose of this study is to define potential circulation and sediment dispersal patterns in the Cretaceous Interior Seaway of North America using a multilayer three-dimensional hydrodynamic model of shallow seas. We present here a series of computer sensitivity experiments in which paleogeography, paleobathymetry, boundary tidal amplitudes, and wind stresses are varied systematically to analyze their effects on circulation. The results of the experiments are hypothetical reconstructions of circulation in the seaway that can be compared with geological observations, thus enhancing our understanding of the hydrodynamic and atmospheric systems that existed in Cretaceous time.

THE MODEL

The circulation model, modified from Leendertse and others (1973, 1975, 1977, 1979) and Liu and Nelson (1977), describes three-dimensional turbulent flow in estuaries and coastal seas. The basic hydrodynamic equations are written for an incompressible fluid on a rotating Earth in Cartesian coordinates with the z-axis directed positive upward (Fig. 1; Table 1; see Table 2 for variable definitions). The first three equations in Table 1 are simplified forms of the Navier-Stokes equations for fluid flow, derived under the following assumptions: (1) the effects of turbulence are included by relating turbulent stresses to mean velocity gradients through an eddy viscosity term; (2) the effects of the Earth's rotation are expressed by a constant Coriolis parameter, f, chosen for a point near the center of the computation field at 45°N (f-plane approximation); (3) vertical motions are dominated by the force of gravity, simplifying the general law of motion in the vertical direction to the hydrostatic approximation; (4) atmospheric pressure gradients are small relative to wind stresses and are not included; (5) the Boussinesq approximation is appropriate; and last, (6) the independent tidal forces on the basin waters are not included. The equation of motion in the z direction (Table 1) is a simplified form of the equation of continuity that assumes the fluid is incompressible, a valid assumption in shallow seas.

Three-dimensional flow structure is simulated by dividing the water column into layers and integrating the system of equations in Table 1 over the height of each layer (Fig. 1), a simplification that greatly reduces computational requirements. The layers are coupled at their surfaces of contact by assuming that the fluid shear stresses above and below a surface are equal (Leendertse, 1977). Vertical eddy viscosity terms and mass exchange coefficients are complex functions of the sub-grid-scale turbulence energy density. A novel feature of the model is that the turbulence energy is generated by interlayer shear and bottom friction, transported like a passive constituent (through an equation similar to the salt equation in Table 1), and dissipated by molecular forces, thereby allowing for dynamic calculation of eddy viscosities. Horizontal mass and momentum exchanges are a function of local horizontal velocity gradients. The equation set is transformed into a finite difference scheme written for a space-staggered grid and is solved implicitly for all variables except the vertical velocity and the horizontal pressure gradients, which are solved explicitly.

Boundary conditions of the circulation model include wind stress at each surface node and water-surface elevations or discharges through time at open boundaries (Table 1). Velocities normal to land along the shoreline are set equal to zero. Initial conditions specified by the user include bathymetry, basin shape, boundary tides, wind speed and direction, current inflows or outflows, water temperature and salinity, and a bed friction factor. Output from the model consists of fluid velocities in three dimensions (u, v, and w components), temperature and salinity, water-surface elevations, tidal ranges, and residual circulation velocities.

The circulation model has been extensively tested (Leendertse and Liu, 1977, 1979) and, for example, reproduces well the three-dimensional flow characteristics of Bristol Bay, a complex, nonhomogenous body of water characterized by strong tidal and wind forcing.

TABLE 3. BOUNDARY AND INITIAL CONDITIONS FOR NUMERICAL EXPERIMENTS OF CIRCULATION IN THE SEAWAY

Experiment	Basin*	Tides†	Wind	Latitude	Figures
1	Alb	20/50	· ·	45°N	· ·
2	Alb	20/50	· ·	60°N	· ·
3	Alb	10/50	· ·	45°N	4
4	Alb§	10/50	· ·	45°N	· ·
5	Alb-TC	10/50	· ·	45°N	· ·
6	Alb	· ·	Winter avg.	45°N	6
7	Alb	· ·	Winter avg.	30°N	· ·
8	Alb	· ·	Winter avg.	60°N	· ·
9	Alb	· ·	Storm type I	45°N	8–12
10	Alb	10/50	Storm type I	45°N	13
11	Alb	· ·	Storm type II	45°N	· ·
12	Tur	20/50	· ·	45°N	· ·
13	Tur**	20/50	· ·	45°N	· ·
14	Tur	10/50	· ·	45°N	4.5
15	Tur-TC	10/50	· ·	45°N	· ·
16	Tur	10/100	· ·	45°N	· ·
17	Tur	10/50	· ·	30°N	· ·
18	Tur††	10/50	· ·	45°N	· ·
19	Tur	· ·	Winter avg.	45°N	· ·
20	Camp	10/50	· ·	45°N	4
21	Camp	10/50	· ·	30°N	· ·
22	Camp	· ·	Winter avg.	45°N	· ·

*Alb = late Albian seaway/ Tur = early Turonian seaway/ Camp = Campanian seaway. TC = basins where transcontinental arch is prominent bathymetric feature.
†North/south boundary tidal ranges in centimeters.
§Chezy factor = 31 $m^{1/2}s^{-1}$.
**Water depth at south entrance to seaway is 200 m.
††Water depths along eastern margin of seaway are 50 m and 25 m.

APPLICATION OF THE MODEL

The Cretaceous Interior Seaway connected the proto–Gulf of Mexico and the Arctic Ocean for ~40 m.y.; during this time, wide variations in several key oceanographic parameters occurred (Kauffman, 1984). Our 22 experiments (Table 3) attempt to bracket these parameters in the following manner.

Paleogeography

Although the shape of the Cretaceous Seaway was always elongate and narrow, as is characteristic of foreland basins, the shoreline configuration varied widely as a function of sedimentation, subsidence, and sea level. Our experiments use three different seaway configurations proposed by Kauffman (1984) and Williams and Stelk (1975) that span the range of potential basin geometries: a seaway of intermediate size during a transgressive peak in the late Albian (T5 of Kauffman, 1984) (Fig. 2A); a seaway of maximum size during transgression (T6) in the early Turonian (Fig. 2B); and a seaway of minimum size at the peak of regression (R8) in the Campanian (Fig. 2C). The blocky outline in Figure 2 reflects the finite difference grid of 70×30×6 nodes in the xyz directions with 111.2 km grid spacing in the y direction, 74.3 km spacing in the x direction, and variable spacing from 25 to 300 m in the z direction.

Paleobathymetry

Numerous authors have used various techniques for estimating paleobathymetry from specific deposits. Williams and Stelk (1975) reported water depths greater than 300 m for upper Turonian deposits in Alberta and British Columbia. Winn and others (1987) estimated depths of 760 ft (232 m) from the Maastrichtian Lewis Shale, whereas Asquith (1970), using clinoforms within the same sequence, provided convincing arguments for water depths of 2,000 ft (610 m). From the clinoforms, Asquith (1970) also estimated that the Lewis shelf along the western margin of the seaway was 100 to 150 mi (161–242 km) wide, with water 200 ft (61 m) deep at the shelf edge. Eicher (1969) used foraminifera from the Greenhorn sequence (lower Turonian) to propose water depths of 1,640 ft (500 m), and alternatively, fluvial paleoslopes to propose depths of 2,000–3,000 ft (610–914 m). More recently, Eicher (1987) suggested that water depths may have been 500 m if the basin relief indicated by paleodrainage patterns in the nonmarine basal Dakota Group did not change after the marine incursion. Estimates of water depth therefore vary widely. Only Kauffman (1977, 1985) proposed a model for the paleobathymetry of the entire basin (Fig. 3). This generalized model for the peak transgressive seaway configuration of the Early Turonian (Figs. 2B and 3) describes an asymmetric bathymetric profile characterized by four "tectono-sedimentologic" provinces: (1) a foreland basin and forebulge zone with water ~50 m deep; (2) an axial basin of maximum subsidence and water depths of 200–500 m; (3) a tectonic hinge zone between the foreland basin and stable platform with water ~100 to 200 m deep; and (4) a stable, shallow, eastern platform of water depths less than 100 m (Kauffman, 1977, 1984, 1985).

In our experiments, we adhere to Kauffman's general paleobathymetric model for the entire seaway and Asquith's analysis for the dimensions of the western shelf. Our western shelf is ~220 km wide and 50 m deep, and maximum

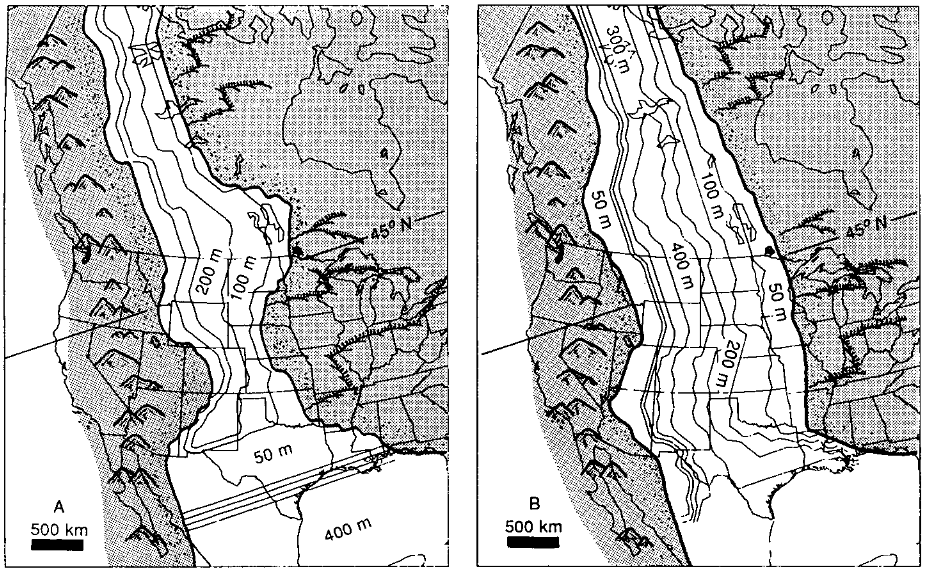

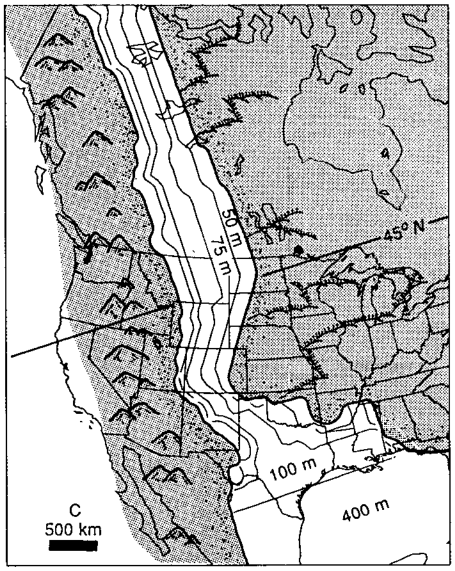

Figure 2. Seaway paleogeographies and paleobathymetries adapted from Kauffman (1984). A. Late Albian seaway during peak T5 transgression. B. Early Turonian seaway during peak T6 transgression. C. Early Campanian seaway during peak R8 regression.

seaway depths are 100 m, 200 m, and 400 m for the Campanian, late Albian, and Turonian seaways, respectively (Figs. 2C, 2A, and 2B). Depths throughout the rest of the basin are scaled down from the maximum depth according to Kauffman's asymmetrical bathymetric profile. In addition, we have included an extensive carbonate bank, with water 50 m deep across the southern entrance of the seaway during the late Albian (Winker and Buffler, 1988; Kauffman, 1984). Seismic profiles across the Gulf of Mexico indicate that this extensive carbonate platform existed during the late Albian but was likely drowned later in the Cretaceous (Winker and Buffler, 1988). The width of the shoal is consistent with Beeson's mapping of carbonate facies during the Albian (D. Beeson, unpub. paleogeographic reconstructions of the seaway).

At times, the transcontinental arch was also an important paleobathymetric structure that influenced deposition in the seaway (Shurr, 1984). We analyzed this influence on the late Albian and early Turonian basins with experiments incorporating a bathymetric arch ~300 km wide, with water 50 m deep, that extended southwest from Lake Superior to the junction of Colorado, Wyoming, and Nebraska (Table 3, experiments 5 and 15).

Bed Friction

The effects of bed friction are introduced into the model by the Chezy coefficient, $C = 0.816\ H^{1/6}\ n^{-1}$, where C is the Chezy coefficient in $m^{1/2}\ s^{-1}$, H is depth in meters, and n is Mannings n in $m^{1/6}$ (Table 1, bed stress equation). Values of C in shallow seas are crude approximations. Csanady (1982) suggested a bottom drag coefficient corresponding to a C of 70 $m^{1/2}\ s^{-1}$. Leendertse and Liu (1975, 1979) used values of 65 and 70 $m^{1/2}\ s^{-1}$ for simulations of the Chesapeake Bay and Bristol Bay, respectively. For our experiments, we use Chezy values of 70, 68, and 60 $m^{1/2}\ s^{-1}$ for the Turonian, late Albian, and Campanian seaways, respectively. These Chezy values correspond to a conservative value for Mannings n of .028 (Slingerland, 1986). We also assessed the effects of greater friction in the seaway by completing experiments with a C of 31 $m^{1/2}\ s^{-1}$ (Table 3, experiment 4).

Tides

This model does not include the effects of independent tides in the seaway, an omission we justify in the discussion of results below. Rather here we investigate the M_2 co-oscillating tidal waves propagating into the seaway from the Arctic and proto–Gulf of Mexico. For the Arctic Ocean, we use open-boundary tidal ranges of 0.1 and 0.2 m in 400 m of water, consistent with present tidal ranges there (Coachman and Aagaard, 1974; Apel, 1987).

Tidal ranges for the southern opening are more difficult to assess because of the uncertain bathymetry of the proto–Gulf of Mexico and the Tethys Ocean. Tidal ranges on modern passive margins such as the North American Atlantic coast are typically 1 m on the outer shelf (Redfield, 1980). Tidal ranges along the modern Gulf Coast, however, which is severely restricted from the open ocean by Cuba, are less than 0.25 m. During the Cretaceous, the Gulf was not as restricted as it is today (Winker and Buffler, 1988), and thus tidal ranges at the southern opening of the seaway were likely to have been between the 1 and 0.25 m ranges described above for modern outer shelves. For this research, we use tidal ranges of 0.5 or 1 m for the southern open boundary of the seaway.

Wind Stresses

Wind stresses are derived from numerical experiments using the National Center for Atmospheric Research (NCAR) Community Climate model (CCM) and Cretaceous paleogeography (Barron and Washington, 1982, 1984; Barron, 1985, 1989). The CCM is a spectral general-circulation model of the atmosphere containing radiation-cloudiness formulations and precipitation-soil moisture, snow cover, and evaporation routines. It satisfactorily simulates many of today's climate characteristics, including observed temperature structure, zonal wind patterns, pressure distribution, and winter storm distributions (Barron, 1989). The Cretaceous experiments consist of two types: mean annual and seasonal. The mean annual experiments incorporate an average annual insolation and an

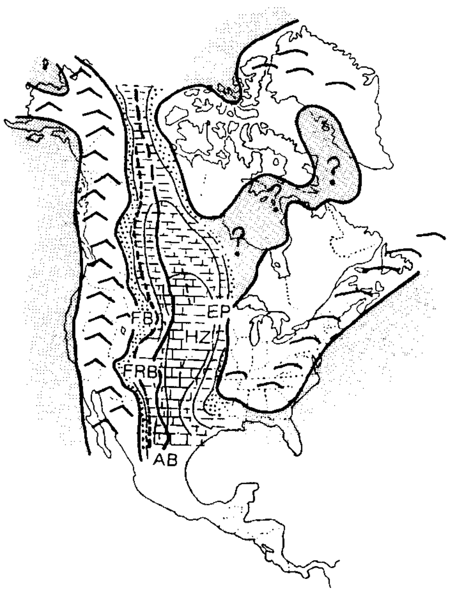

Figure 3. Kauffman's (1977, 1984, 1985) bathymetric model of the Cretaceous Interior Seaway during the early Turonian consisting of four major tectono-sedimentologic zones: (1) foreland basin (FB) and forebulge (FRB) zone with water depths rarely greater than 50 m; (2) axial basin (AB) of greatest subsidence and water depths (200–500 m); (3) hinge zone (HZ) with water 100–200 m deep; (4) shallow eastern platform (EP) with water depths less than 100 m. (Modified from Kauffman, 1985.)

energy-balance ocean that does not account for heat storage, transport, and diffusion. The seasonal model accounts for changing daily insolation, and ocean seasonal heat storage (Barron, 1989). The solar insolation is that produced by present-day, Milankovitch orbital parameters. Experiments using insolation maximized or minimized for summer in the Northern Hemisphere (Thomas Glancy, 1989, personal commun.) indicate that storm tracks change very little as a function of this parameter. Atmospheric conditions, or the weather, are computed by the CCM every 12 hr.

For this study, wind fields generated by three different Cretaceous climate simulations, each assuming present-day levels of atmospheric CO_2, were available to us (E. J. Barron, 1989, personal commun.): (1) a mean annual simulation for the late Albian; (2) a mean annual simulation for the Campanian; (3) a winter seasonal simulation for the late Albian. We experimented with five types of wind stresses derived from these three simulations: average mean annual winds for the late Albian, average mean annual winds for the Campanian, average winter winds for the late Albian, and two winter storms for the late Albian. The average mean annual winds are 100-day averages of winds computed every 12 hr during a mean annual CCM experiment. Maximum winds are only 1 to 2 m s^{-1}, too small to drive circulation and sediment transport in the seaway. The average winter winds are a 90-day average of winds computed during December, January, and February of a seasonal CCM experiment. Maximum winds are 5 to 7 m s^{-1}, sufficiently strong and organized to drive circulation. Using summer winds was also an option, but summer winds are weaker and less consistent than winter winds. In this paper, therefore, we present results using winds generated by the winter seasonal simulation.

The Cretaceous Interior Seaway is not fully connected in the late Albian CCM experiments; three land grid points separate the northern and the southern arms of the seaway. This difference of three grid points between a connected and unconnected seaway, however, would likely have no effect on the CCM-computed atmospheric circulation (E. J. Barron, 1989, personal commun.).

The U (easterly) and V (northerly) components of wind velocity computed by the CCM for the lowermost model level (about 0 to 70 m above the Earth's surface) are converted to surface wind stresses that drive the hydrodynamic model by way of the wind stress equation in Table 1. C^*, the drag coefficient, is experimentally determined for wind speeds usually measured at a reference elevation of 10 m above the surface. Typical wind profiles for the Earth's surface indicate that mean wind velocities for 70 m above the surface differ little from velocities

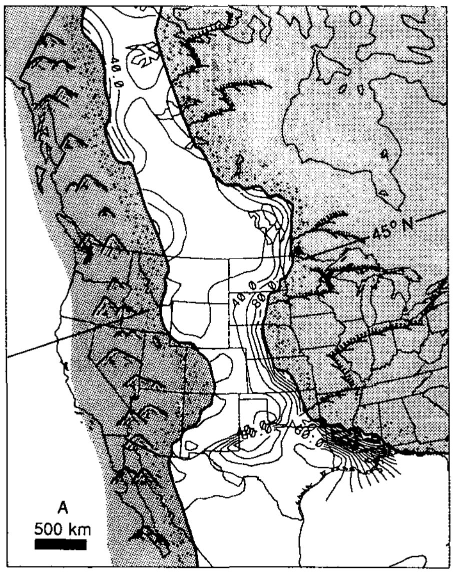

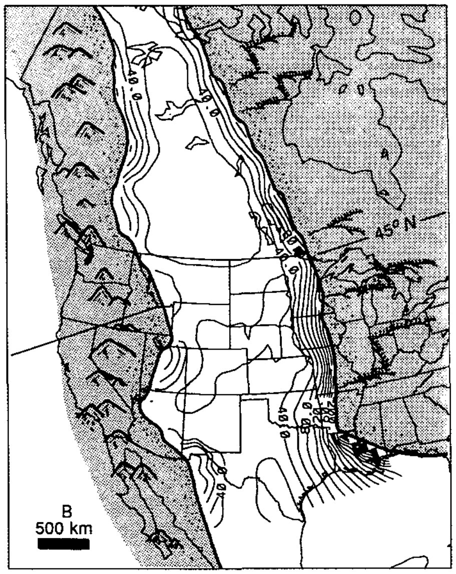

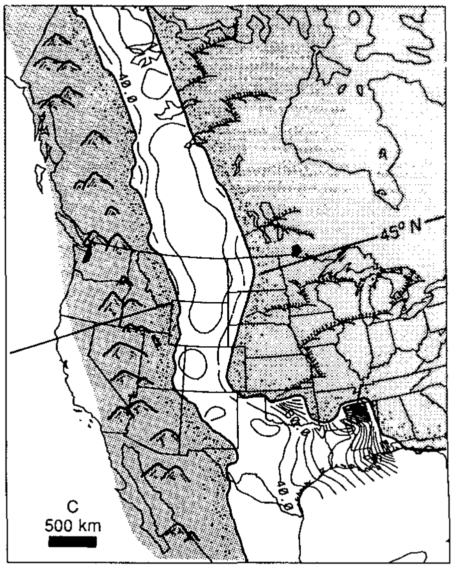

Figure 4. Tidal ranges computed over one tidal cycle for three basin configurations: A. late Albian, B. early Turonian, and C. early Campanian. Boundary tidal ranges are 0.1 m at the Arctic opening and 0.5 m at the southern opening. The contour interval is 20 cm. Microtidal ranges are computed everywhere except along the southeastern coast where ranges are mesotidal to macrotidal.

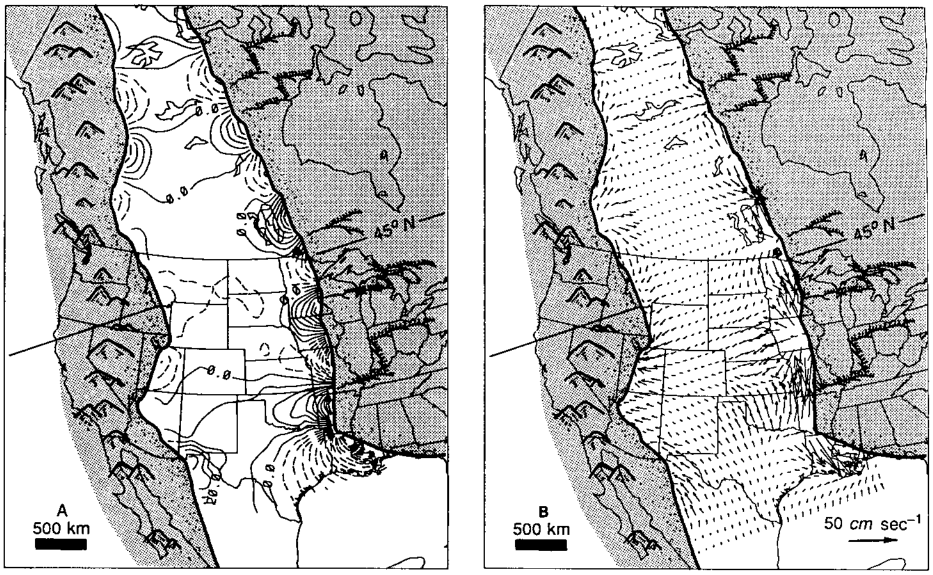

Figure 5. Snapshots of the water-surface elevations (A) with respect to still water, and surface-water (0–25 m) currents (B) in the early Turonian seaway during high tide at the open boundaries. The contour interval is 10 cm; dashed lines are negative surface elevations.

measured at 10 m (Gill, 1982). The CCM computed wind velocities therefore are converted to shear stresses, using standard drag coefficients in the literature. For our experiments, we used a C^* of 1×10^{-3} for wind speeds less than 10 m s^{-1}, and a C^* of 2×10^{-3} for wind speeds greater than 10 m s^{-1} (Pond and Pickard, 1983).

Stratification

In the experiments presented in this paper, the water column is unstratified. Although oxygen- and carbon-isotope studies (Kauffman, 1984; Wright, 1987; Barron and others, 1985) indicate that at times the seaway was stratified, we believe that stratification is not critical for simulations using winter winds. Along the Atlantic shelf during the winter, the water column is unstratified because sea-surface temperatures decrease, and the more intense winter winds increase mixing (Swift and Niederoda, 1985; Swift and others, 1986b). We assume that this seasonal cycle of stratification also occurred in the Cretaceous Interior Seaway. Even if the seaway were stratified, however, preliminary simulations including a stably stratified water column indicate that the results are not qualitatively different.

The 22 different combinations of these parameters in Table 3 encompass what we believe are the most probable boundary and initial conditions for the seaway. We simulated approximately four days of circulation in the seaway with each of these combinations of input parameters, using an IBM 3090-600E vector computer at the Cornell National Supercomputer Facility. Each experiment required an average of 1 hr of CPU time at Cornell, or the equivalent of ½ hr with a Cray X-MP processor.

RESULTS AND DISCUSSION

All references to direction in the following discussion are in paleo-coordinates, and the five lakes in Canada that parallel the axis of the seaway (see Fig. 2) are used for location. From north to south, these lakes are Great Bear Lake, Great Slave Lake, Athabaska Lake, Reindeer Lake, and Lake Winnipeg.

Tides

Tidal ranges computed in experiments 3, 14, and 20 (Table 3) for the three different basin configurations are presented in Figure 4. The predicted tidal ranges for the different paleogeographies and bathymetries, while differing in magnitude, all show the higher ranges along the southeastern and northwestern coasts. The explanation for this pattern is made more apparent by observing the computed water-surface elevations and surface-layer currents for the Turonian run (Fig. 5), at the moment of high tide at the southern entrance. Apparently the tides act as progressive (versus standing) waves and are deflected to the right by Coriolis forces (in the Northern Hemisphere). The co-oscillating tidal waves from the south propagate up the east side of the basin, the waves from the north propagate down the west side, and there is limited interaction between the two. These are classic Kelvin waves, topographically trapped by the Coriolis force along the coast (Csanady, 1982). Because there is little interaction between the two wave trains and little reflection of the waves off the sides of the basin, they act as progressive waves propagating at a speed, or celerity, $C^2 = gH$ where g is gravity and H is depth. The waves along the east coast propagate at a speed of 22 m s^{-1} corresponding to a depth of 50 m along the eastern, shallow platform, and have a wavelength of ~1,000 km (Fig. 5A). The water along the west margin of the seaway is deeper, and thus the wave speed is 25 m s^{-1}, and the wavelength is 1,100 km.

The closest modern counterpart exhibiting this type of tidal regime is the North Sea. It is rectangular in shape, open to the ocean along its entire north side, broad enough that cross-basin oscillations are eliminated, influenced by a strong Coriolis force, and dominated by an M_2 co-oscillating tide entering from the north (Defant, 1958). The southern end of the North Sea is open only through the narrow Straits of Dover, which transmit little tidal energy. The M_2 tide from the Atlantic is a progressive Kelvin wave that travels south along the western side of the basin with as much as 3 m of amplitude, rotates counterclockwise along the (effectively) closed southern end, is frictionally damped, and then travels north along the eastern edge with amplitudes of less than 0.3 m (Defant, 1958; Nihoul, 1982).

Second-order differences among the three simulations (Figs. 4A, 4B, and 4C) are the result of differing paleogeographies and bathymetries. During the late Albian, (Fig. 4A) the extensive shoal at the southern opening of the seaway frictionally damped the tidal energy entering the seaway from the Tethys. Although reflection of energy is also a possibility, a tidal wave traveling in 200 to 400 km of water has a wavelength of 2,000–2,700 km, which is too great to be reflected by a shoal 50 m deep and 500 km long (Koutitas, 1988). The model thus predicts co-oscillating tidal ranges during this interval of only 1 m north of the shoal in the United States, and less than this north of the United States–Canadian border (Fig. 4A). Similarly, during the R8 regression in the Campanian, with a maximum water depth of 100 m, the tidal wave is largely damped by friction, and minor ranges of 0.5 m are predicted everywhere north of the Oklahoma embayment (Fig. 4C). On the other hand, during the Turonian, when the shoal probably did not exist (Kauffman, 1984; Winker and Buffler, 1988), and when water depths within the seaway were likely greater, from those proposed by Slater (1985) and Ryer and Kauffman (1980). Slater concluded that the independent tides, rather than co-oscillating tides, were the dominant tides in the seaway, even during periods when there was unrestricted tidal communication between the proto–Gulf of Mexico and the seaway. Slater's most realistic model, using a uniform depth of 200 m, yields maximum tidal ranges of 0.9 m and maximum currents of 0.1 m s^{-1}. These results include the very strong effects of basin resonance at a basin average depth of 211 m. Any change in basin depth away from the resonance depth dramatically reduces his computed independent tidal ranges; his computed maximum tidal ranges for basins 100 m and 600 m deep are less than 0.1 m and 0.3 m, respectively. Our experiments, on the other hand, indicate that the co-oscillating tides from the north may have resulted in tidal ranges of nearly 1 m along the northwest shelves, and that even during times of severe restriction in the late Albian and Campanian, the co-oscillating tide from the south may have resulted in larger tidal ranges along the southeast margins (Fig. 4). During times of unrestricted flow between the seaway and the proto-Gulf, such as the peak T6 transgression of the early Turonian, co-oscillating tides almost certainly were much greater than the maximum independent tides computed by Slater. Maximum independent tides, therefore, are equivalent in magnitude to co-oscillating tides only for our Campanian basin configuration. This is due to severe restriction of co-oscillating tides from the proto-Gulf in our experiments, and significant augmentation of independent tides due to basin resonance in Slater's experiments. For other basin configurations, co-oscillating tides are clearly dominant.

Ryer and Kauffman (1980) proposed that tides in the seaway were augmented as they propagated north along the southwest coast and that they attained mesotidal ranges in Wyoming and Montana. Conversely, our results indicate that the southwestern and central western shoreline was microtidal. This is consistent with the observations of Thorne and Swift (1985) and suggests that tidal deposits described along the southwestern shoreline are the product of localized amplification in channels and bays.

In summary, the tidal experiments allow the following conclusions.

1. Co-oscillating tides propagated into the Cretaceous Interior Seaway as progressive Kelvin waves. The eastern margin of the seaway was influenced by tides propagating north from the Tethys Ocean, whereas the western margin of the seaway was influenced by tides propagating south from the Arctic Ocean. This is in opposition to tides in many modern epeiric seas such as the Yellow and Arafara (Klein and Ryer, 1978), where tides exhibit both standing and progressive characteristics, thereby becoming augmented at certain points in their interiors.

2. Maximum tides of mesotidal to macrotidal range are predicted in the southeastern corner of the seaway.

3. For Late Albian and Campanian paleogeographies, the model predicts insignificant tides in the seaway north of Texas; maximum ranges are nearly 1 m along the northwest margin in Canada.

4. For the early Turonian paleogeography, when there was unrestricted flow between the seaway and the proto-Gulf, our experiments indicate that tidal ranges were much greater in all parts of the seaway than for late Albian or Campanian paleogeographies. The model pre-

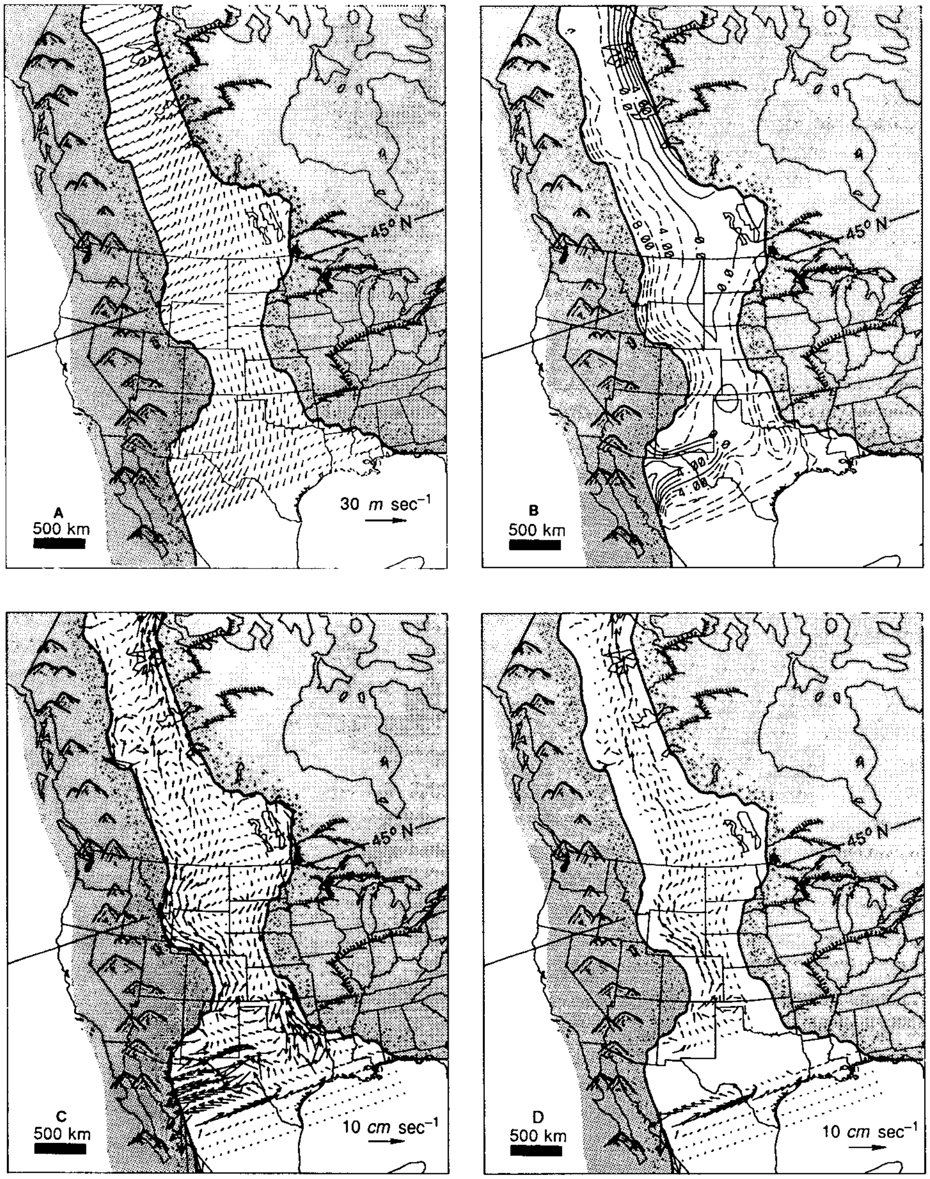

Figure 6. Circulation and set-up generated in the late Albian seaway by average winter winds. A. Average winter winds computed over the seaway in a seasonal CCM experiment for late Albian paleogeography. Note that in these and the subsequent storm experiments, each CCM computed wind vector is mapped to a 5 by 7 block of nodes in our model. In all of the vector plots, grid points are located at the tails of each arrow, and the length of the arrow and size of the arrowhead increase linearly with velocity. B. Steady-state water-surface elevations. Contour interval is 2 cm; dashes are negative values. C and D. Steady-state, vertically averaged currents computed in the upper 25 m (C), and in 50–100 m of water (D).

ranges of 1.8 m and maximum velocities of 0.3 m s^{-1} are predicted into Minnesota, and ranges of 1.2 m extend well into northern Canada (Figs. 4B and 5B). An additional experiment (Table 3, experiment 13) indicates that the larger Turonian tidal ranges are not sensitive to decreasing depths from 400 m to 200 m at the south entrance of the seaway.

Computed tidal ranges along the northwestern margin of the seaway in Canada are remarkably similar for the Turonian and Albian basins, ~1 m, with maximum velocities of only 0.1 m s^{-1} (Figs. 4 and 5B). Again, this arises from the Arctic co-oscillating boundary tide propagating as a Kelvin wave down the western margin of the seaway. Because the geometry of the seaway in the north did not vary as extensively as the geometry in the south (Kauffman, 1984), tidal characteristics along the northwestern coast also did not vary greatly. Computed tidal ranges for the shallower Campanian basin are slightly smaller because of frictional damping (Fig. 4C). Increasing the Arctic boundary tidal ranges to 20 cm increases computed tidal ranges along this northwestern coastline by ~50% (Table 3, experiments 1, 2, 12, and 13). Farther south, along the western margins of the seaway in the United States during the late Albian (Fig. 4A) and Campanian (Fig. 4C), tidal ranges are insignificant. Only for Turonian paleogeography does the model compute ranges of ~1 m along the southwestern coasts of the seaway (Fig. 4B). This is probably due to the greater water depths (maximum of 400 m) of the Turonian experiment, which reduces frictional damping of the tidal wave from the north and increases tidal ranges resulting from the co-oscillating tide from the south. Yet even during the Turonian, maximum velocities in this part of the seaway are less than 0.2 m s^{-1}.

All three experiments predict maximum tidal ranges along the southeastern coast of the seaway in Mississippi, Oklahoma, and Arkansas. Tidal ranges are augmented eight to twelve times above the boundary range of .50 m, and reach as much as 4 to 6 m, with corresponding velocities of 0.6 m s^{-1}. Two factors probably contribute to this augmentation: (1) deflection due to the Coriolis force and (2) convergence. Because the tides hug the sides of the basin, resonance is probably important in augmenting tides only in relatively narrow embayments such as the Mississippi Embayment during the Campanian (Fig. 4C). Deflection due to the Coriolis effect can be estimated using a simplified equation for geostrophic balance that assumes steady flow and negligible bottom friction:

$$V = \frac{g}{f}\frac{\partial \zeta}{\partial x} \quad (1)$$

TABLE 4. DEPOSITS FROM THE CRETACEOUS INTERIOR SEAWAY THAT EXHIBIT TIDAL INFLUENCE

Rock unit	Age	Location	References
(1) Fall River Fm.	Early Albian	Northeast Wyoming	Campbell and Oaks (1973)
(2) Moosebar and Gates Fm.	Albian	Fort St. John, British Columbia	Leckie and Walker (1982) Carmicheal (1988)
(3) Viking Fm.	Late Albian	Southwest Saskatchewan	Evans (1966)
(4) Viking Fm.	Late Albian	Central Alberta	Reinson and others (1988)
(5) Viking Fm.	Late Albian	Southwest Alberta	Leckie (1986)
(6) Dakota Gp.	Late Albian	Denver, Colorado	MacKenzie (1972)
(7) Ferron Sandstone, Mancos Shale	Turonian	Castle Valley, Utah	Cotter (1975)
(8) Virgelle Mbr., Milk River Fm.	Early Campanian	South Alberta	Leckie and others (1989)
(9) Eagle Sandstone	Early Campanian	North-central Montana	Rice (1980)
(10) Spring Canyon Mbr., Blackhawk Fm.	Campanian	Helper, Utah	Kamola and Howard (1983)
(11) Mesaverde Fm.	Late Campanian	Sand Wash Basin, Colorado	Masters (1967)
(12) Almond Fm.	Late Campanian	Rock Springs, Wyoming	Weimer (1966)
(13) Horseshoe Canyon and Bearpaw Fms.	Campanian-Maastrichtian	Drumheller, Alberta	Rahmani (1988)
(14) Oak Canyon Mbr., Dakota Ss	Cenomanian	White Mesa, New Mexico	Nummedal and Swift (1987)

where V is velocity in the y direction, g is gravity, f is the Coriolis parameter (1.03×10^{-4} for 45°N lat.), and $\partial\zeta/\partial x$ is the water-surface gradient in the x direction (Csanady, 1982). This equation yields a water-surface gradient of 7.36×10^{-7} in geostrophic balance with an average open boundary tidal velocity of 0.07 m s^{-1}. Remarkably, this gradient is only one order of magnitude less than the gradient of the tidal wave itself—8.9×10^{-6} for a tidal wave of amplitude .25 m in 400 m of water. This geostrophic gradient means that the water will pile up to a water-surface elevation of 1.05 m at the east end of the south boundary, and thus accounts for 25% of the amplification.

The convergence effect between two sites (1 and 2) can be estimated using Green's Law:

$$\frac{a_1}{a_2} = \left(\frac{l_2}{l_1}\right)^{½}\left(\frac{h_2}{h_1}\right)^{¼} \quad (2)$$

where a is tidal amplitude, l is shelf length, and h is water depth (Slingerland, 1986). The tidal augmentation due to decreasing water depth from 400 m to 50 m, with no crest convergence, is $a_2 = 1.7a_1$. Assuming a_1 is the tidal amplitude of 1.05 m adjusted for the Coriolis deflection yields an augmentation of 1.76 m. The sum is a tidal range of 3.52 m and accounts for most of the maximum tidal range computed by the hydrodynamic model. The remainder of the tidal augmentation is likely due to convergence of the crest.

The results presented in Figure 4 are relatively insensitive to the range of Coriolis forces spanned by the Cretaceous Seaway. As mentioned above, our model assumes a constant Coriolis force corresponding to 45°N latitude. To investigate the sensitivity of these results to the range of Coriolis forces spanned by the seaway, we conducted three additional experiments (Table 3, experiments 2, 17, 21) using Coriolis forces corresponding to 30°N and 60°N latitudes. The tidal ranges computed in these experiments differ only slightly from the previous runs. The effects of increasing the magnitude of the Coriolis force to the north would be to increase slightly the magnitude of the Kelvin wave as it propagates to the north, and to decrease the magnitude of the Kelvin wave as it propagates to the south. In contrast, the results are quite sensitive to the Chezy friction coefficient. Computed ranges along the southeast margin of the late Albian Seaway are reduced 30% to 40% when greater bed friction is simulated using a Chezy factor of 31 $m^{½} s^{-1}$ (Table 3, experiment 4). The friction represented by this Chezy factor, however, is excessive—much greater than that assumed by Leendertse and Liu (1975, 1979) in successful simulations of Bristol Bay and Chesapeake Bay.

The transcontinental arch, extending from Lake Superior to the junction of Colorado, Wyoming, and Nebraska, is reported to have influenced deposition in the seaway (Shurr, 1984). Our experiments (Table 3, experiments 5 and 15), however, suggest that an arch 300 km wide with water 50 m deep did not significantly alter the main features of tidal circulation in the Albian and Turonian basins.

Taken altogether, these experiments suggest a different characterization of tidal regime in the Cretaceous Interior Seaway of North America dicts ranges of as much as 2 m along much of the seaway's southeastern coast in the United States and 1- to 1.5-m ranges along the southwest coast.

5. Co-oscillating tides, for most combinations of basin geometry and bathymetry, were probably the dominant contributor to tides in the seaway. Independent tides were equal in magnitude to co-oscillating tides probably only when the basin resonated with the independent tide-producing forces, and when the southern opening of the seaway was severely restricted to co-oscillating tides.

Wind-Driven Circulation

Both steady-state winds and temporally varying winter storms were applied to the seaway. Experiments using simple steady-state winds were conducted first, and served three main purposes: (1) to assess dominant mechanisms controlling wind-driven circulation in the seaway, (2) to analyze the influence of different basin geometries and bathymetries on wind-driven circulation, and (3) to explore the sensitivity of the computations to the Coriolis effect. The storm experiments, on the other hand, represent possible basin responses to the dominant sediment-transporting events in the seaway. Our assumption is that these storm experiments best reflect the long-term, sediment-transport directions and currents for the emplacement of "event beds" on the seaway's shelves.

Steady-State Winds. To analyze the response of the three different seaways to the same wind field, we applied to each an average winter-wind field generated by the NCAR CCM for a late Albian paleogeography (Table 3, experiments 6, 19, and 22). The seaway response (Fig. 6) is dominated by coast-constrained, shore-parallel currents in geostrophic balance, similar to those observed on the North American Atlantic shelf (Swift and others, 1986a). This behavior arises because (1) the continuity principle restricts water movement into or away from the shore; thus, close to the shore, the water flows in the direction of the longshore component of the wind. (2) The Coriolis force deflects surface-layer flow to the right of the wind in the Northern Hemisphere, resulting in Ekman drift. For winds blowing in a direction such that the coast is to the right, water is deflected and piles up landward. The resulting pressure gradient in turn drives underlying water offshore that is deflected to the right and alongshore by the Coriolis force. This type of flow, where the pressure gradient is balanced by the Coriolis force, is called "geostrophic flow." (3) Conservation of vorticity maintains flow parallel to bathymetric contours. Along the western shelf north of Colorado and south of Great Slave Lake, and along the northeastern shelf, east- and northeast-trending winds of 5 to 7 m s^{-1} (10 to 14 knots) drive currents of nearly 0.1 m s^{-1} predominantly shore-parallel, but with a slight orientation in the direction the wind is blowing (Fig. 6C). Ekman transport generates a maximum water surface set-up of 0.13 m along the northeast coast between Great Slave Lake and Great Bear Lake that drives currents in the subsurface layers directly parallel to bathymetric contours (Fig. 6D). The computed results are consistent with equation 1 wherein an average shelf velocity of 0.05 m s^{-1} along the northeastern shelf in the vicinity of Great Bear Lake (Fig. 6C) is in geostrophic balance with a cross-shelf gradient of 5.26×10^{-7}, or a set-up of ~0.12 m over 230 km. This compares well with the model computed set-up of 0.13 m.

Along the shelf in the far northwest corner of Canada, northwest and west of Great Bear Lake, currents are directed south, in opposition to the general circulation pattern. This illustrates the key role the shores play in constraining circulation in narrow basins. The wind stress in this area is directed east-southeast, contrary to the east-northeast winds over the rest of the northern seaway (Fig. 6A). Because the longshore component of the wind is to the south, therefore, the resultant current is shore-parallel to the south. This also illustrates the sensitivity of the circulation to wind direction relative to the coastline. A more southerly trend of only a few degrees in the wind can reverse the general basin response.

Northward currents along the western coast of Colorado oppose weak southward winds because they are responding to the large-scale water-surface gradient. Water is flowing to the north toward the maximum set-down along the Wyoming-Montana shelves. South of Colorado, southwest-trending winds drive strong westward currents of up to 0.15 m s^{-1}. Computed current velocities are greater in this part of the seaway because the water is only 50 m deep over the carbonate platform, and the average winds are stronger because they are influenced by the regular equatorial easterlies.

The computed water-surface elevations and currents for the Turonian and Campanian seaways (Table 3, experiments 19 and 22) generally are similar to those discussed above, thereby illustrating the controlling influence of the coasts on the flows. There is one notable difference, however, because the early Turonian seaway during the peak of the T6 transgression was much wider than the late Albian and Campanian seaways. In the center of the model seaway, the shorelines are sufficiently far removed such that surface velocities are dominated by Ekman drift and are to the right of the wind, to the south in the northern part of the basin. In contrast, the Campanian and the late Albian seaways are sufficiently narrow such that currents are predominantly shore-parallel.

These results are not sensitive to the range of Coriolis forces applicable to the Cretaceous Seaway. Experiments completed for the late Albian Seaway using the same winter winds but with Coriolis forces corresponding to 30°N and 60°N latitude (Table 3, experiments 7 and 8) show little difference in the general-circulation pattern and surface-elevation pattern generated in the seaway.

In summary, two main conclusions emerge from these experiments using winter-average winds. First, circulation is controlled mainly by geostrophic balance and coastline-constrained

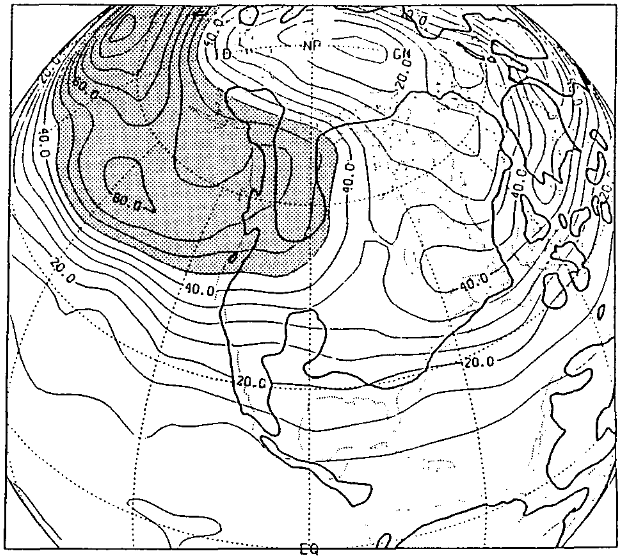

Figure 7. CCM-predicted Cretaceous winter storm tracks over North America as indicated by the time-filtered, standard deviation of the geopotential height field in meters at 500 millibars. See text for details (E. J. Barron, 1989, written commun.).

currents generally flowing parallel to the shoreline and bathymetric contours. Only during maximum flooding in the early Turonian are shorelines far enough removed for Ekman drift to control surface circulation in the center of the basin. The tendency of currents to flow shore-parallel also implies that computed circulation would differ little if we used a smooth wind field that varied with each node, rather than the 5 by 7 "blocks" of wind apparent in Figure 6A. Second, wind-driven circulation is relatively insensitive to the range of Coriolis forces spanned by the seaway.

Storm-Driven Circulation. Both hurricanes and winter storms were probably important agents in forming storm deposits in the Cretaceous Interior Seaway (Duke, 1985; Barron, 1989), but because hurricanes are too small to be resolved in the CCM grid, we restrict our analysis to extra-tropical winter cyclones. The most probable winter storm track across the seaway was obtained from the time-filtered, standard deviation of the geopotential height field at 500 millibars (Barron, 1989) (Fig. 7). Geopotential height describes the amount of work required to bring a parcel of air to sea level. Large deviations in the geopotential height field indicate large variations in atmospheric pressure. When filtered for time periods typical of winter storms, large standard deviations of the height field, such as the shaded region in Figure 7, should indicate the passage of numerous winter storm systems. Two types of storm systems can be identified by visual inspection of the near-surface wind velocities: (1) tightly wound and well-organized storms (storm type I), with at least four days of winds significantly greater than average, representing an average winter storm or sediment-transporting event in the seaway, and (2) an extreme event (storm type II) with the greatest wind speeds computed by the CCM during 100 days of winter.

Storm Type I. Our example is visible in Figure 8 as a large counterclockwise rotating air mass over North America spanning ~20 degrees of latitude. As such, it is slightly larger than a typical winter storm on the Middle Atlantic Bight that spans 15 degrees of latitude (Vincent, 1986). The maximum wind speeds of nearly 20 m s^{-1}, however, are similar to wind speeds during typical winter storms on the Atlantic coast. The storm moves approximately due east along the path defined in Figure 7, and thus stresses the water through nearly 360 degrees.

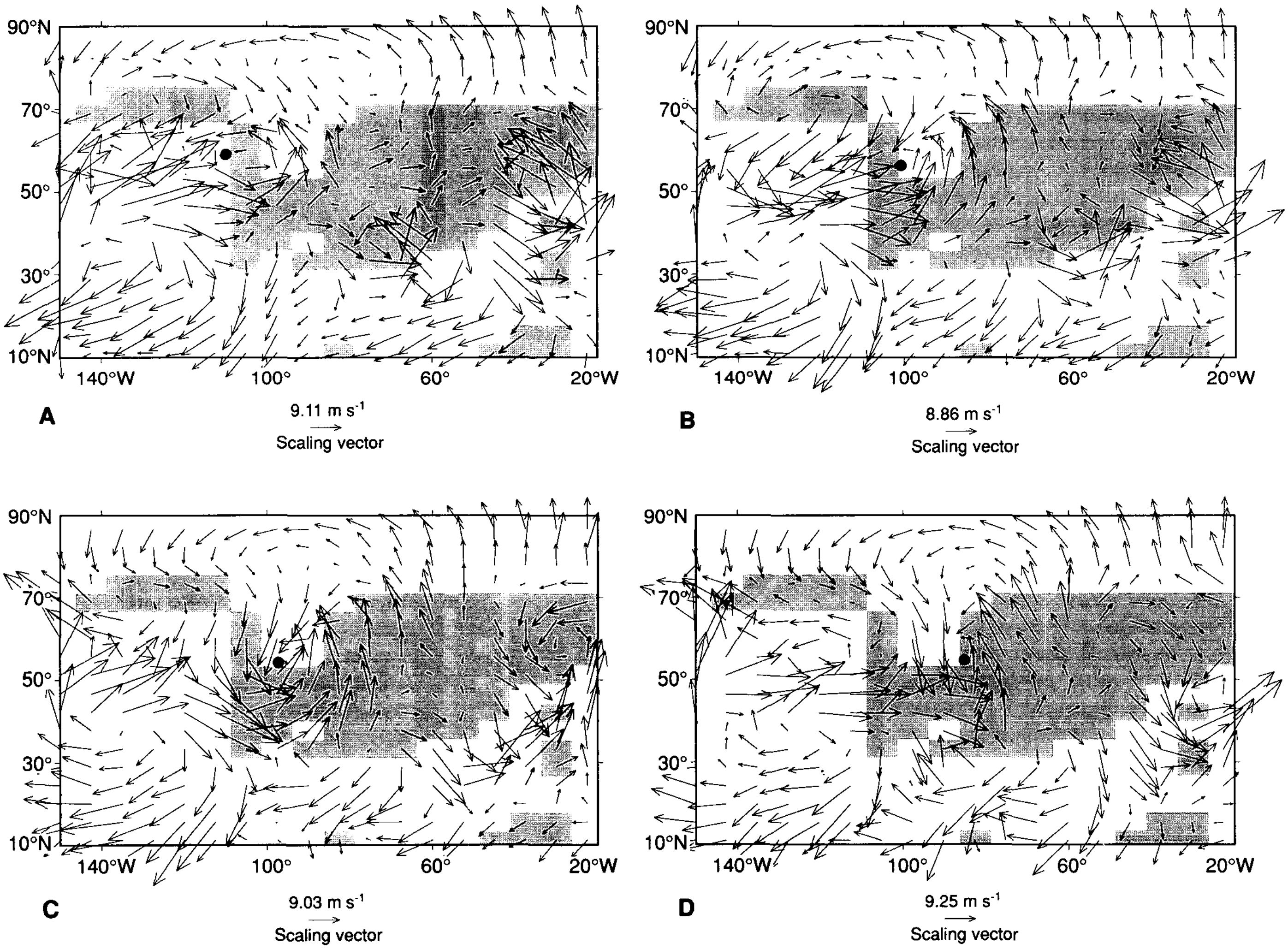

Figure 8. Storm type I. Velocity vectors during a four day (A–D) winter storm computed over North America in a CCM seasonal experiment using late Albian paleogeography. Surface winds (0–70 m) flow counterclockwise around the storm center (black dot) with maximum speeds of nearly 20 m s^{-1}. The large screened area in each part represents the outline of North America during the late Albian transformed onto the CCM grid of 4.5° latitude by 7.5° longitude. The Western Interior Seaway, in the center of each figure, is not connected for the CCM experiment. Scale is in m s^{-1} (E. J. Barron, 1989, written commun.).

During the first day, the storm center is west of the seaway, and southerly winds dominate, reaching maximum speeds of 17.5 m s^{-1} (35 knots) (Figs. 8 and 9A). The corresponding water-surface elevations are similar in pattern, although much larger in magnitude, to the elevations computed using winter average winds (compare Figs. 6B and 9B). The water surface is set up nearly ½ m along the northeastern coast, and set down nearly ¾ m along the Idaho-Wyoming coast (Fig. 9B). Circulation, therefore, is strongest and shore-parallel along these same coasts, reaching maximum speeds of 0.25 m s^{-1} on the shelves (Fig. 9C), 0.15 to 0.18 m s^{-1} at 50- to 100-m depth (Fig. 9D), and 0.09 m s^{-1} in the basin thalweg.

During the second day, the storm center is approximately on the western margin of the seaway (Fig. 8B). Winds in the central portion of the seaway remain southerly with maximum speeds of 15 m s^{-1} (30 knots), but winds in the northern portion of the seaway have shifted, blowing to the west and slightly south (Fig. 10A). Thus, the most notable change from day 1 is the generation of shore-parallel currents to the south on the northwestern shelf in response to the more northerly winds in the area (Fig. 10C). Farther offshore, in 100 m of water, currents are still predominantly to the north (Fig. 10D). The shifting winds along the northeastern coast also have caused (1) water-surface set-ups to decrease and shift slightly to the south (Fig 10B) and (2) current velocities to decrease to 0.16 m s^{-1}. Along the Wyoming-Montana shelf, set-down is less, with maximum currents of 0.23 m s^{-1}.

During the third day of the storm, winds in the northern part of the seaway blow strongly to the southwest, but winds in the central portion continue to blow northward (Figs. 8C and 11A). Consequently, the water surface is set up 0.45 m along the northwestern shelf (Fig. 11B) in geostrophic balance with south-directed currents (Fig. 11C). The maximum set-down, now 0.74 m, remains in Wyoming and Montana, whereas the set-up along the northeastern shelf has shifted farther to the south near Lake Winnipeg. Currents along the northeastern margin of the seaway remain isobathyal to the north at speeds of 0.27 m s^{-1}, counter to the wind in the far north, creating a counterclockwise circulation system. Northern-directed currents are still computed in Montana, causing flow to converge at the Canada-Montana border. In 100 m of water, maximum currents of 0.27 m s^{-1} are predicted in Wyoming (Fig. 11D).

The center of the storm during the fourth day has moved east fully across the seaway (Figs. 8D and 12A), causing northerly winds in the northern part of the seaway, whereas winds over the mid-section are westerlies. This initiates a dramatic shift in circulation; flows are to the south over most of the seaway (Figs. 12C and 12D). Maximum computed water velocities are 0.27 m s^{-1} over the shelves, and 0.18 m s^{-1} at 100-m depth. The water-surface gradients are in geostrophic balance with the northerly currents with a set-down of 0.6 m along the northeastern coast and a set-up of up to 0.45 m along the western coast (Fig. 12B). In general, basin response to the storm has completely reversed relative to the first two days. Although somewhat counterintuitive, these results are not without an analogue. Water-surface set-ups of 0.6 m and geostrophic currents of 0.4 m s^{-1} are frequently observed on the Atlantic Shelf during a winter storm (Swift, 1986a), and reversals of both are not uncommon (Lee and others, 1985; Butman and others, 1979).

Parrish and others (1984) computed storm circulation over the Campanian shelf in Wyoming and Montana, using wind stresses applied uniformly over the region. Their computed storm flows are predominantly to the south and contour-parallel. The shore-parallel flows they computed are consistent with our results, but

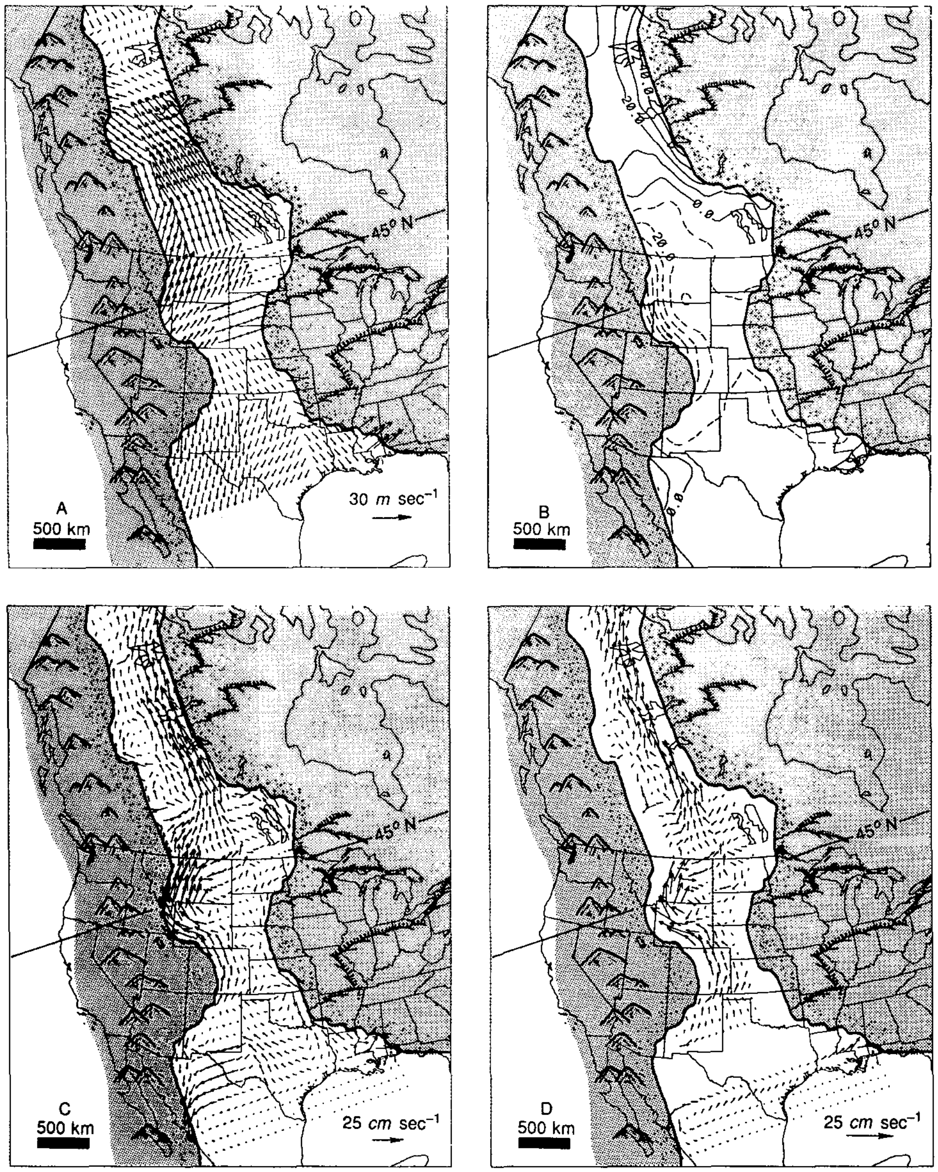

Figure 9. Storm type I winds and water-surface elevations and circulation after the first day of the storm. A. CCM-computed wind vectors transferred onto our more detailed grid and paleogeography. B. Computed water-surface elevations in 10-cm contour intervals. C and D. Computed currents in surface 25 m of water (C), and 50–100 m of water (D).

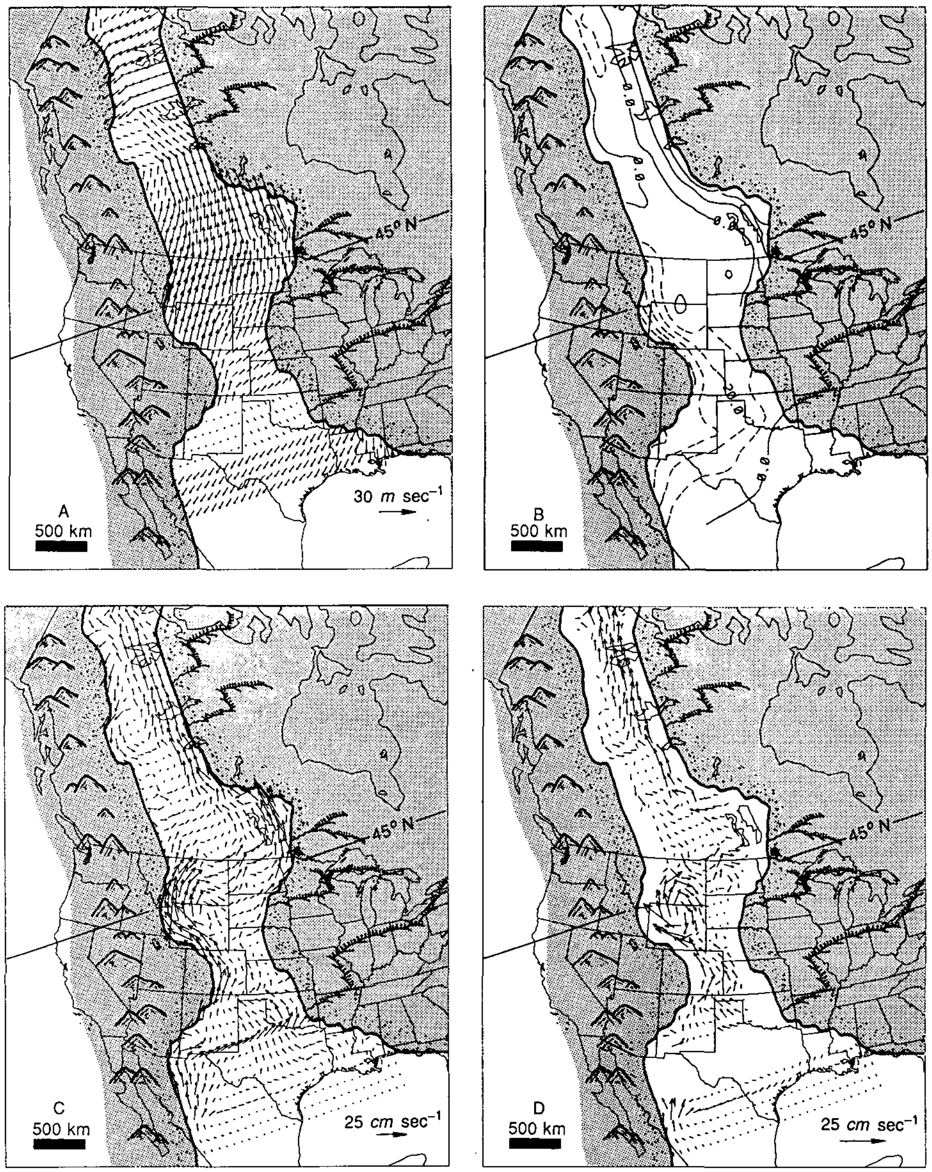

Figure 10. Storm type I winds and water-surface elevations and circulation after the second day of the storm. A. Storm winds transformed into our more detailed grid and paleogeography. B. Computed water-surface elevations in 10-cm contour intervals. C and D. Computed currents in surface 25 m of water (C), and 50–100 m of water (D).

our results also suggest that it is not sufficient to apply uniform wind stresses to the seaway. As discussed above, the passage of a winter storm stresses the seaway with a wide range of winds and drives strong flows both to the north and the south.

Our discussion so far has omitted wind-generated water-surface waves. They are important because their orbital velocities are superimposed on the flows presented here and because in the nearshore they generate longshore currents through radiation stresses. Maximum wave heights and periods generated in the seaway during this storm can be estimated using existing wave hindcasting methods; we focus this discussion on the western coast because its deposits are better studied. The Darbyshire-Draper method (Koutitas, 1988) predicts that 20 m s^{-1} winds blowing for more than 12 hr and over distances greater than 300 km will create deep-water waves with significant heights of 5.5 m and periods of 11 s. Significant wave heights are the average of the highest one-third of the waves. The corresponding wavelength of these waves is 188 m; the waves feel the bed, therefore, in water shallower than 94 m. The equivalent significant wave heights and periods predicted by this method in water only 40 m deep are 4.9 m and 9 s, respectively. These values differ only slightly from the deep-water calculations, implying that wind-driven waves of these periods in water deeper than 40 m have little energy extracted by bed friction.

As the storm passes across the seaway, the northerly winds of day 4 are probably the major source of high-energy waves along the western shoreline. By virtue of being at the tail end of the storm, these winds and the waves they induce would last longer because they are not immediately countered by winds blowing in the opposite direction. The North Atlantic shelf along the eastern United States again is a suitable modern analogue. Strong winter winds are from the northwest and the northeast. Winds from the northwest, however, because they blow offshore, do not produce large waves at the shore; storm winds from the northeast, on the other hand, blow onshore and generate high waves (U.S. Army CERC, 1975; Niedoroda and others, 1984). For these reasons, the resulting dominant longshore currents and net sediment-drift directions are to the south (Komar, 1976). At Wallops Island, Virginia, for example, from 1945 to 1957 winds blew from directions between north-northeast and east-southeast (the quadrant from which waves must propagate to induce longshore drift to the south) less than 20% of the time (Slingerland, 1977). Yet longshore currents and net sediment drift are to the south, both because winds from these directions are more intense than onshore winds from the south and because intense winds from the northwest blow offshore and do not produce significant waves. We conclude that net longshore drift along the northwestern shores of the Cretaceous Interior Seaway should have been to the south.

All of the results discussed above were obtained in the absence of tides, and the question arises whether this is a serious omission. Figure 13 presents the surface layer circulation computed after day 3 of the same storm, but with tides included. Comparing Figures 13 and 12C reveals that north of Colorado and Kansas the circulation patterns generally are equivalent in both experiments, although current magnitudes may be slightly greater or smaller, depending on tidal interaction. In the southernmost part of the seaway, however, the circulations are different, reflecting the stronger influence of tides and the weaker influence of winds there. This suggests that circulation in the seaway during the late Albian was tide-dominated in the southeast and storm-dominated in the middle and northern segments.

Storm Type II. This storm contains the maximum winds (28 m s^{-1} or 56 knots) computed over the seaway by the CCM. It is less well

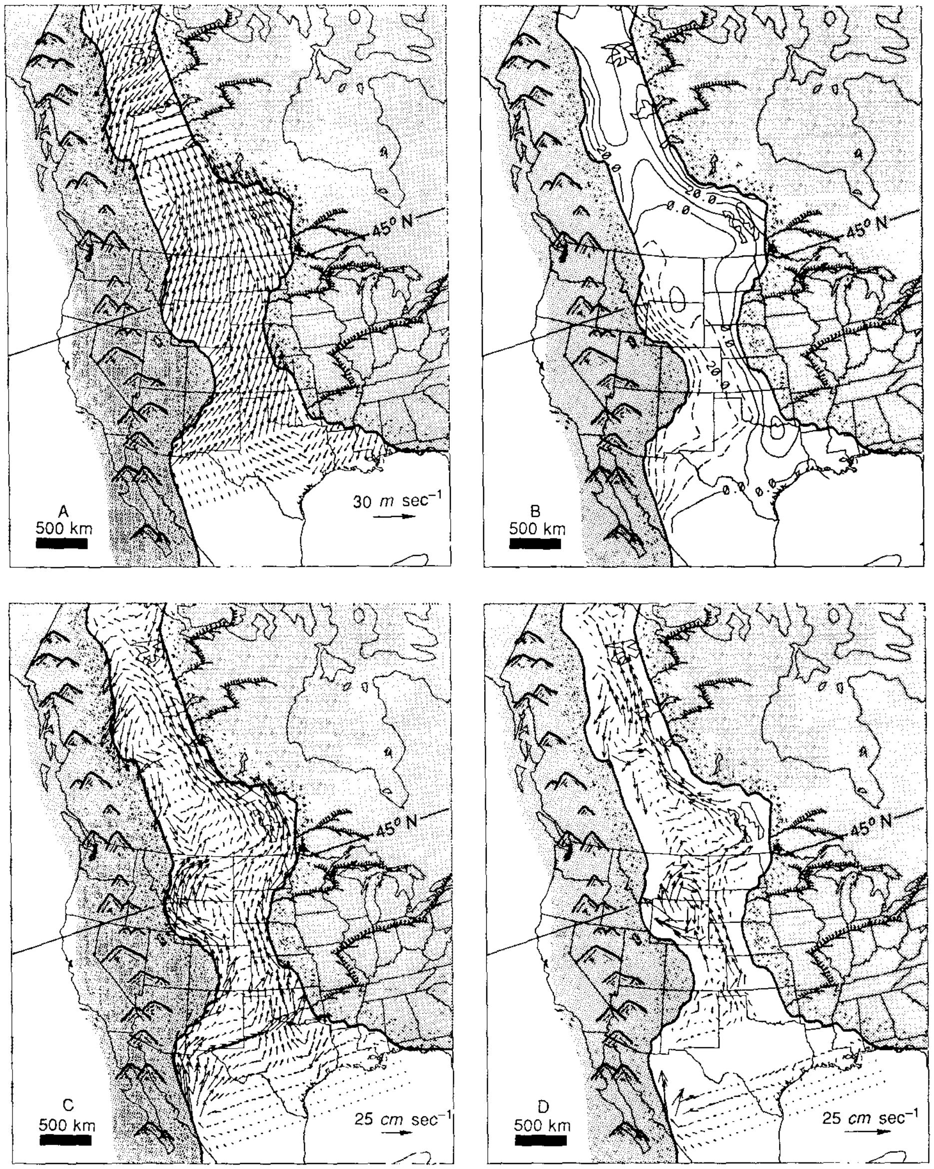

Figure 11. Storm type I winds and computed water-surface elevations and circulation after the third day of the storm. A. Storm winds transformed into our more detailed grid and paleogeography. B. Computed water-surface elevations in 10-cm contour intervals. C and D. Computed currents in surface 25 m of water (C), and 50–100 m of water (D).

organized than Storm Type I, has a more northerly track, and does not have a coherent rotating flow that drives strong northerly winds on the trailing side. Only results for the fourth day of the storm are discussed here, because winds are so weak on the first day that no significant currents are generated, and responses of the second and third days are quite similar to the basin's response to winter average winds, but magnified.

During the fourth day of the storm, the dominant winds over the seaway remain strongly to the north from Wyoming to Canada and have intensified to a maximum velocity of 28 m s^{-1}. Computed water-surface elevations and currents have increased commensurately, reaching maximums of 1.8 m and 0.8 m s^{-1}, respectively, over the northeastern shelves.

This more extreme response of the seaway, when compared to the results from storm type I, warrants an explanation. First and most obviously, wind velocities are greater. Second, winds are consistently in one direction. Third, shore-parallel winds can generally produce greater set-ups and currents than onshore or offshore winds. This is not intuitive and is best explained using simplified equations for shore-parallel winds and water set-ups that assume negligible bottom friction (Csanady, 1982):

$$U = \frac{U_*^2}{f}\left(1 - e^{\frac{x}{R}}\right) \tag{3a}$$

$$V = U_*^2 t e^{\frac{x}{R}} \tag{3b}$$

$$\zeta = \frac{U_*^2}{f\sqrt{gH}}\left(f\,t e^{\frac{x}{R}}\right) \tag{3c}$$

where U_*^2 is longshore wind stress (m^2 s^{-2}), U and V are cross-shore and longshore transport, respectively (m^3 s^{-1} per unit width), t is time (s) f is the Coriolis parameter (s^{-1}), ζ is water-surface elevation close to shore (m), x is cross-shore distance, zero at the shore, less than zero away from shore (m), H is depth (m), g is gravitational acceleration (m s^{-2}), and R is a radius of deformation equal to $\sqrt{gH}/f$, or 210 to 430 km in our model. Close to shore ($x/R < 1$), U approaches 0, V approaches $U_*^2 t$, and the water-surface set-up approaches $\zeta = U_*^2\, t/\sqrt{gH}$ or $V/\sqrt{gH}$ (Csanady, 1982). Thus, close to shore, in the absence of bottom friction, the wind simply accelerates the water, and V increases linearly with time. The water surface set-up in geostrophic balance with V also increases linearly with time and thus can be much larger than the case for an onshore wind. Of course, in reality, bottom friction balances these forces, but only after greater set-ups and velocities have been generated than in the case for onshore-trending winds.

The computed reponse of the seaway to the type II storm is similar in pattern, but more severe, than the response of the Atlantic shelf to a scale-matching winter storm such as the storm of March 22, 1973, described by Swift and others (1986a). For several days during this storm, winds of 15 to 30 m s^{-1} blew to the south, approximately parallel to the shoreline of the Middle Atlantic Bight. Consequently, the water surface was set up 0.6 m along the entire coast, driving a massive geostrophic flow of 0.4 m s^{-1} for several days. Our computed set-ups and currents are substantially greater than those reported for the Atlantic shelf, probably because winds in our experiment are stronger for a longer period of time, and because longitudinal winds in the Cretaceous Seaway drive strong flows over both east and west shelves, thereby mobilizing the entire water mass.

The experiments discussed above using winter storms have three important limitations. First, our results do not include hurricanes, although they were probably important in the Cretaceous Interior Seaway, particularly in the southern part. Barron (1989) suggested that hurricanes were common during the Cretaceous, but that during the Early Cretaceous the zonal nature of atmospheric circulation would have directed

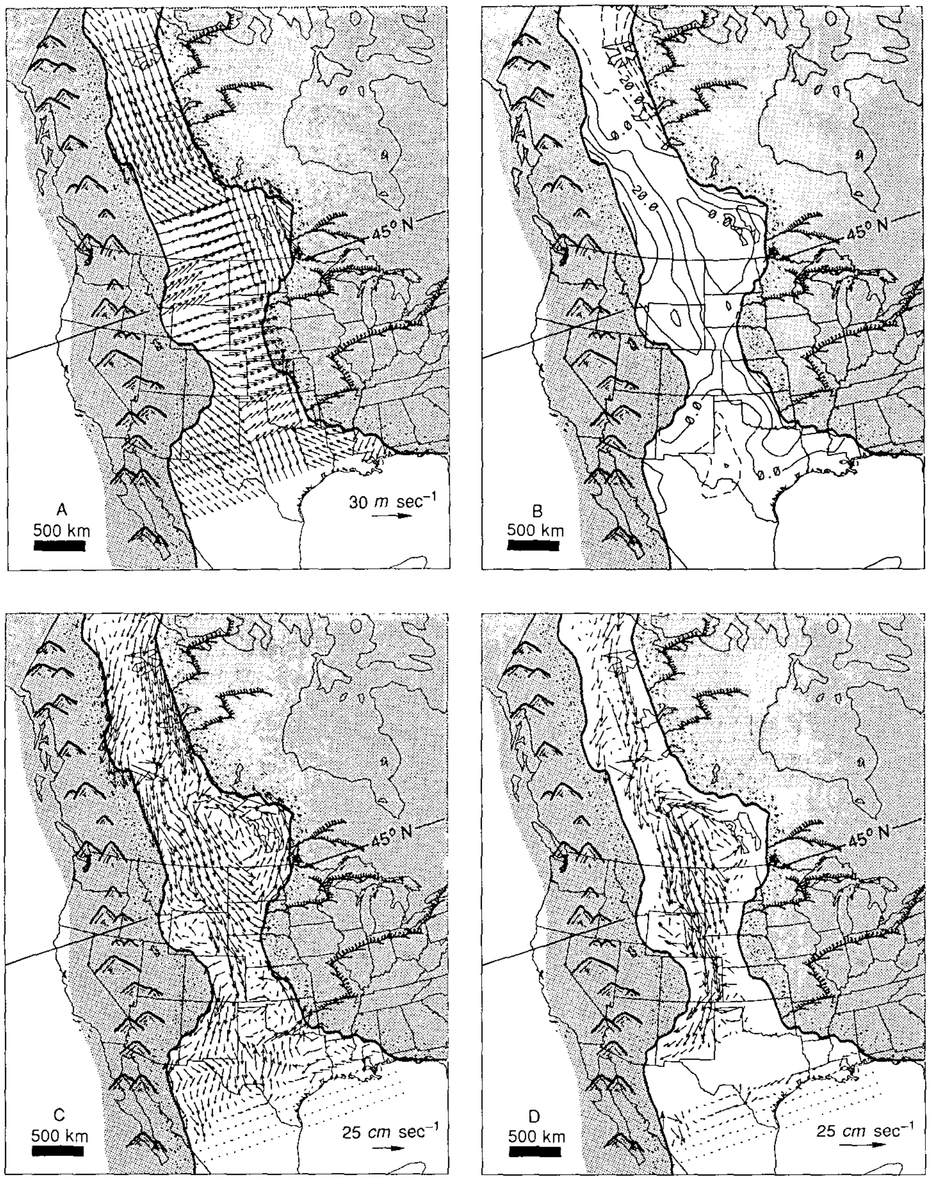

Figure 12. Storm type I winds and computed water-surface elevations and circulation after the fourth day of the storm. A. Storm winds transformed into our more detailed grid and paleogeography. B. Computed water-surface elevations in 10-cm contour intervals. C and D. Computed currents in surface 25 m of water (C), and 50–100 m of water (D). The center of the storm has moved east fully across the seaway, causing wind to blow from the north, down the axis of the northern part of the seaway. Basin response to the storm has completely reversed relative to the first two days.

most of these hurricanes into the Pacific. During Late Cretaceous time, however, the North Atlantic was large enough to disrupt zonal circulation patterns, and hurricanes may have been steered into the Cretaceous Seaway. The circulation generated by hurricanes would probably have been similar to that generated by winter storms—coast-constrained, geostrophic, and thus, generally shore-parallel. But the tracks of hurricanes would have been different. They would have entered the seaway from the south, and to penetrate northward, would have moved along the axis of the seaway. Such a hurricane would drive flows to the south along the western margin of the seaway and to the north along the eastern margin, and would have been less likely to produce reversing flows.

Second, our results do not account for the effects of stratification. Our assumption that the basin was unstratified during the winter is probably reasonable over the shelves but is speculative for deeper parts of the basin. The extent to which strong storms can destratify a basin is unclear and worth additional investigation.

Third, our results use winds generated by a CCM experiment assuming present-day levels of atmospheric CO_2. These CCM experiments, however, do not fully account for the high Cretaceous temperatures indicated by paleoclimate data, and increased atmospheric CO_2 may be required to account for the elevated temperatures (Barron, 1984). Yet seasonal Cretaceous climate experiments have not been completed using increased atmospheric CO_2. If higher levels of CO_2 shift only predicted storm tracks, then basin response to the storms would be similar to that presented in this paper, only shifted appropriately in space. If higher levels of CO_2 significantly alter the nature and strength of the computed storms, then the resulting basin circulation would also be significantly different.

With these qualifications, the following conclusions arise from the experiments using winter storms:

1. A coherent mid-latitude cyclone passing entirely across the basin stresses the water with a nearly 360° range of wind directions. During the first stage of the storm, winds generate currents predominantly to the north, and the water surface dips westward. Toward the end of the storm, this response is completely reversed, such that currents are predominantly to the south, and the water surface dips eastward. The predominant paleocurrent imprint from such a storm should be shore-parallel to the south, with occasional records of bidirectional, opposing currents. Along the western coast, winds from the north at the end of the storm may have generated southward, propagating waves 4.9 to 5.5 m high with 10-s periods that drove associated longshore drift to the south.

2. More extreme winds could produce shore-parallel currents of up to .80 m s^{-1} with maximum set-ups and set-downs of 1.80 m and 1.65 m, respectively, and deep-water waves 8 to 9 m high with periods of 14 s.

3. Winter storms in the CCM simulations rarely pass south of Colorado. If the storms we simulated are representative of winter storms during Cretaceous time, then our experiments show that circulation in the seaway, and consequently resulting deposits, were likely storm dominated in the northern and middle sections of the seaway and tide dominated along the southeastern coast. Again, this conclusion considers only winter storms passing over the seaway. If hurricanes frequently passed into the seaway, then our argument that circulation was storm dominated would be strengthened, and

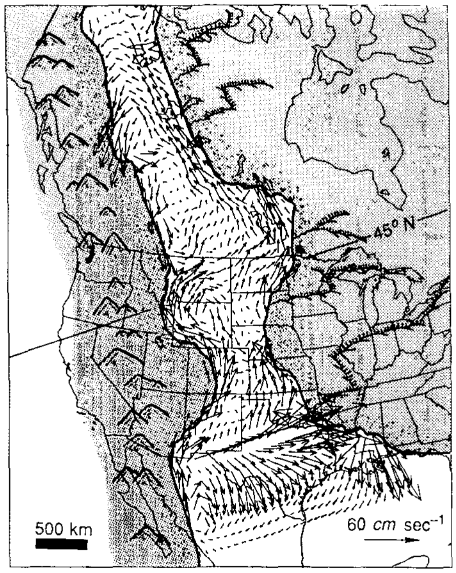

Figure 13. Surface layer circulation computed after the third day of storm type I, including tides. Compare with Figure 11C. North of Colorado and Kansas, the circulation patterns generally are equivalent. The similarity in all but the southernmost portion of the seaway suggests that the circulation in the seaway was storm dominated.

would perhaps even apply to the southeastern coast also.

COMPARISON OF RESULTS WITH GEOLOGIC OBSERVATIONS

The simulations discussed above yield several hypotheses that can be compared with observations and interpretations from the geologic record.

1. Circulation in the Cretaceous Interior Seaway, in general, was dominated by storms everywhere except along the southeastern coast.
2. Meso- to macro-tidal ranges occurred along the southeastern coast, whereas microtidal ranges prevailed in the rest of the seaway.
3. Storm-driven shelf currents were shore-parallel, predominantly to the south, but occasionally to the north.
4. Longshore currents and net sediment drift were to the south along the northwestern coast.

Below, we compare these hypotheses with published geologic observations and interpretations summarized in Figure 14 and Tables 4 and 5. To present these data, we had the option of combining it for all time periods onto one map containing our early Turonian shoreline configuration, or presenting the data for a particular time period on a separate map with the temporally appropriate seaway shoreline. We chose the first option because the exact shoreline configuration corresponding to each deposit is uncertain. Some deposits therefore could have been presented with inappropriate shoreline configurations, and those deposits that did not correspond to an available shoreline configuration would be excluded. Second, the orientation of the western shoreline north of Texas in our early Turonian basin mirrors trends that existed throughout much of the seaway's history (Kauffman, 1984; D. Beeson, unpub. paleogeographic reconstructions of the seaway). Data combined on this map adequately reveal the information we need to compare the data with our model results. Figures 14A and 14B display the locations of deposits described as exhibiting tidal influence and storm influence, respectively. Storm influence is indicated by hummocky cross-strata, and by trough and tabular cross-strata in shelf sandstone ridges interpreted in the literature as produced by storm-driven shelf flows. The citations of hummocky cross-strata are largely those tabulated by Duke (1985) but also include more recent citations. Tables 4 and 5 list the names, ages, locations, and references corresponding to these deposits.

The types of severe storms responsible for the deposits presented in Figure 14 and Table 5 cannot be confidently inferred because the diagnostic imprints of different storm types on deposits are unclear. Duke (1985) inferred a hurricane origin for most of the hummocky stratified deposits but also admitted that a winter-storm origin cannot be ruled out. For this study, we assume that the deposits are simply indicators of severe storms, and we conclude that the computed response of the basin to winter storms is consistent with the nature of the deposits. We have not modeled the response of the basin to hurricanes, however, and thus the nature of the deposits may also be compatible with a hurricane origin. This is a particularly strong possibility in the Grayson Formation in northeastern Texas (no. 2 in Fig. 14B and Table 5) which has been interpreted by Hobday and Morton (1984) as a storm-dominated unit, within our inferred tide-dominated setting.

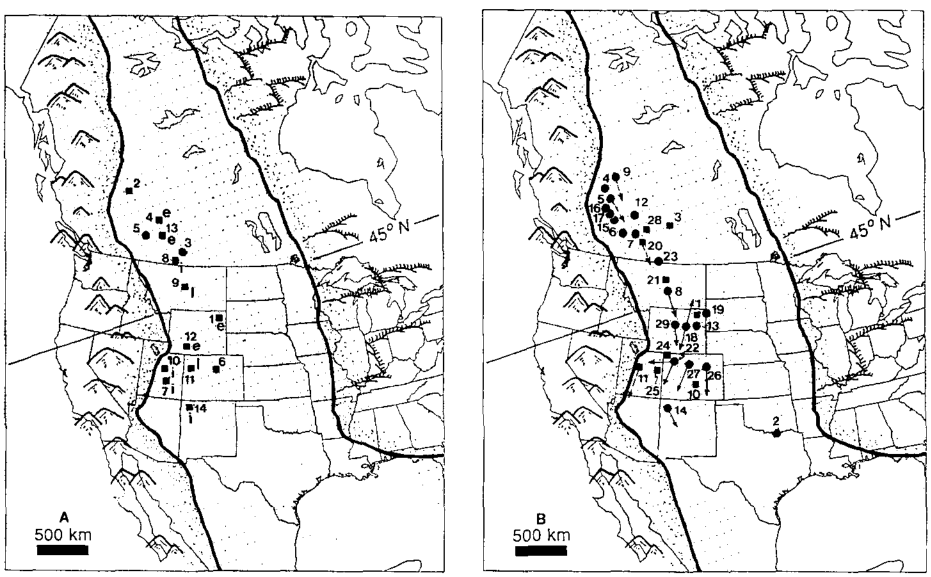

Figure 14. Locations of deposits from the Cretaceous Interior Seaway that exhibit tidal influence (A), and storm influence (B). Dots indicate offshore deposits; squares indicate coastal deposits. e = estuarine, i = tidal inlet, l = lagoonal. Solid arrows show shelf paleocurrent directions, primarily derived from trough and tabular cross-strata or grain-size trends. Dashed arrows show longshore drift directions. The deposit names, ages, locations, and references are listed in Tables 4 and 5.

Circulation Was Dominated by Storms

A comparison of Figures 14A and 14B reveals that there are many more deposits from the Cretaceous Interior Seaway interpreted as storm influenced than as tidally influenced. Secondly, of the 14 deposits cited as exhibiting tidal influences, 10 were interpreted as occurring in sheltered environments such as lagoons, estuaries, and tidal inlets, and only 4 were interpreted as occurring in a shelf environment. Conversely, we found descriptions of 19 storm-influenced

TABLE 5. DEPOSITS FROM THE CRETACEOUS INTERIOR SEAWAY THAT EXHIBIT STORM INFLUENCE

Rock unit	Age	Location	References
(1) Fall River Fm.	Early Albian	Northeastern Wyoming	Campbell and Oaks (1973)
(2) Grayson Fm.	Early Albian	Northeastern Texas	Hobday and Morton (1984)
(3) Mannville Gp.	Early Albian	Lloydminster, Saskatchewan	Lorsong (1982)
(4) Moosebar and Gates Fms.	Albian	Fort St. John, British Columbia	Leckie and Walker (1982)
(5) Cadotte Mbr., Peace River Fm.	Middle Albian	Northwestern Alberta	Rahmani and Smith (1988)
(6) Viking Fm.	Late Albian	Southwestern Alberta	Leckie (1986)
(7) Dunvegan Fm.	Cenomanian	Eastern Alberta	Duke (1985)
(8) Mosby Sandstone, Belle Fourche Shale	Cenomanian	Central Montana	Rice (1984)
(9) Doe Creek Mbr., Kaskapau Fm.	Cenomanian	Peace River, Alberta	Wallace-Dudley and Leckie (1988)
(10) Codell Sandstone, Carlile Shale	Middle Turonian	Pueblo, Colorado	Duke (1985)
(11) Ferron Sandstone, Mancos Shale	Turonian	Castle Valley, Utah	Cotter (1975)
(12) Cardium Fm.	Late Turonian	Central Alberta	Duke and others (1980), Duke (1981)
(13) Frontier Fm.	Late Turonian	Powder River Basin, Wyoming	Winn and others (1987)
(14) Gallup Sandstone, Mancos Shale	Coniacian	Northwestern New Mexico	Campbell (1971)
(15) Marshybank Mbr., Wapiabi Fm.	Santonian	South Alberta	Duke (1985)
(16) Chungo Mbr., Wapiabi Fm.	Santonian	South Alberta	Duke (1981)
(17) Wapiabi–Belly River Transition	Early Campanian	Southwestern Alberta	Duke (1981)
(18) Shannon Sandstone, Cody Shale	Early Campanian	Salt Creek, Wyoming	Spearing (1976), Tillman and Martinsen (1984), Gaynor and Swift (1988)
(19) Sussex Sandstone, Cody Shale	Early Campanian	Northeastern Wyoming	Berg (1975)
(20) Virgelle Sandstone, Milk River Fm.	Early Campanian	South Alberta	Leckie and others (1989)
(21) Eagle Sandstone	Early Campanian	North-central Montana	Rice (1980)
(22) Duffy Mountain Sandstone, Mancos Shale	Early Campanian	Northwestern Colorado	Boyles and Scott (1982b)
(23) Milk River and Lea Park Fms.	Campanian	Southeastern Alberta, southwestern Saskatchewan	Meijer Drees and Myhr (1981)
(24) Mesaverde Group	Campanian	Northwestern Colorado	Boyles and Scott (1982a)
(25) Spring Canyon Mbr., Blackhawk Fm.	Campanian	Book Cliffs, Utah	Howard and others (1982)
(26) Hygiene Sandstone	Campanian	Denver Basin, Colorado	Harms and others (1982) Kiteley and Field (1984)
(27) First Mancos Sandstone, Mancos Shale	Campanian	Northwestern Colorado	Kiteley and Field (1984)
(28) Horseshoe Canyon and Bearpaw Fms.	Campanian-Maastrichtian	Eastern Alberta	Rahmani (1988)
(29) Sandstones in Mowry Shale	Albian	North-central Wyoming	Davis and Byers (1989)

sequences deposited in an offshore setting. Additionally, there is only one occurrence of inferred reversing tidal flows set within an estuarine setting, among dozens of storm-dominated coastal sequences in the Cardium Formation (W. L. Duke, 1989, personal commun.). Published geological interpretations thus strongly confirm our hypothesis that storm-generated waves and currents were the dominant processes emplacing sand beds in offshore settings. This agreement between modeling results and geologic data also implies that the CCM–computed atmospheric circulation during winter over North America is consistent with field data as well. Tides were important primarily in environments sheltered from storm waves and currents, particularly in estuaries and shoreline embayments where convergence and resonance could strongly amplify regional tidal ranges. Two citations where offshore tidal deposits are described occur in Alberta, where our model predicts relatively large tidal ranges for the western coast of the seaway. A third citation occurs in northwestern New Mexico where local shoaling amplification or resonance may occur at a scale unresolved by our model.

To argue that circulation in the seaway was dominated by storms requires that one assume that fair-weather winds did not play a significant role in sedimentation. Robert W. Frey has pointed out (1989, personal commun.) that the Spring Canyon Member of the lower Campanian Blackhawk Formation in Coal Creek Canyon, Utah, is often cited as a storm-dominated shelf sequence, but it contains only 7% by volume of obvious event beds. Does the other 93% of the section reflect fair-weather sedimentation? We think not, because sediment transport is a power function of flow intensity, and predicted flow intensities in the seaway are very low for the average wind fields discussed above. Possibly these finer-grained sediments were emplaced by less intense storms.

Tidal Ranges Were Mesotidal and Macrotidal along the Southeastern Coast, but Microtidal Everywhere Else

As Figure 14A illustrates, this hypothesis is not supported by geological observations. There are several potential reasons for the discrepancy. First, data and outcrops are limited along the former eastern shorelines of the seaway; the western margin, on the other hand, has abundant outcrop and subsurface data, and it has been extensively studied because of its hydrocarbon resources. Second, tidal ranges entering the seaway from the Tethys may have been much smaller than the 0.5-m range we assumed. This explanation would probably also imply that the Campeche and Florida escarpments were effective barriers to tidal energy, resulting in a proto–Gulf of Mexico during Cretaceous time that was nearly as restricted from open ocean tides as the Gulf is today. We believe this is unlikely considering that sea level during the Cretaceous is estimated to have been 300 m greater than sea level today (Kauffman, 1984). A smaller boundary tidal range would reduce tides along the southwestern coast, and create a discrepancy with observed tidal deposits in that area.

Third, it is possible that the eastern shelf of the seaway was substantially shallower than the 100 and 50 m depths we assumed, and thus it rapidly damped tidal energy. To test this premise, we performed an additional model experiment for the Turonian basin, assuming that water over the eastern platform was 50 and 25 m deep (Table 3, experiment 18). This shallow eastern margin reduces computed tidal ranges in the southeastern corner of the seaway nearly 50% relative to our standard Turonian experiment (Fig. 4B). Tides computed along the eastern margin south of Reindeer Lake, however, are still significant, ranging between 1 and 2 m. The eastern margin would need to be substantially shallower than 50 and 25 m to damp out tides.

Lastly, the Cretaceous Seaway was nearly always silled across the southern boundary. The experiments we completed using the Albian and Campanian basins illustrate that either a constricted opening (Fig. 4C), or a shallow platform across the opening (Fig. 4A) dramatically diminishes tidal ranges along the eastern margins. Distributions of paleobiogeographic units, however, indicate that the southern opening of the seaway was unrestricted for significant periods of time, particularly during sea-level highstands (Kauffman, 1984). A silled southern opening cannot be a complete explanation for the absence of tidal evidence along the eastern margin.

In the absence of adequate data from the southeastern portion of the seaway, we believe that the most plausible explanation for the discrepancy between our model results and geologic observations is either that tides were significant along the eastern margin, but that a lack of data hides the evidence, or that tides were damped by a shelf with water depths much shallower than 25 m.

Storm-Driven Shelf Currents Were Shore-Parallel, Predominantly to the South, Occasionally to the North

Figures 8–13 illustrate that a winter storm passing across the seaway will initially drive currents on the western shelf shore-parallel to the north but will ultimately generate shore-parallel currents to the south. We suggest that winter-storm deposits should record mainly this final southward flow, but might also occasionally record northward flows. Studies of high-angle cross-strata in shelf-sandstone bodies (Fig. 14B; Table 5) deposited in the seaway support this hypothesis. The dominant transport direction, indicated by tabular and trough cross-strata or fining of grain size, is shore-parallel to the south (nos. 8, 14, 18, 22, 26, 27, 29; Fig. 14B). In the Shannon Sandstone (no. 18; Fig. 14B), however, a minority of the cross strata indicate directly opposing, northward, shore-parallel flows, consistent with our predictions. Nearly all of the paleocurrents illustrated in Figure 14B are reported to be shore-parallel. The northeast-southwest orientations in Colorado, Wyoming, and Utah simply mirror a similarly trending coastline in those states (Figs. 2B and 2C) throughout much of the history of the seaway (Kauffman, 1984; D. Beeson, unpub. paleogeographic reconstructions of the seaway).

Our conclusions are in direct contradiction to those of Leckie and Krystinik (1989), who used sole marks of hummocky cross-stratified beds, parting lineation, and combined flow ripples to argue that there is no evidence for geostrophic currents preserved in the Cretaceous Blackhawk, Moosebar, and Gates Formations where they have examined them in British Columbia and Utah. They maintain that sediment transport was always directly offshore. We avoided these paleocurrent indicators in our discussion above, because as Duke (in press) has pointed out, these features probably form as a result of *instantaneous* flow conditions within an inner boundary layer, which in turn results from the superimposition of waves and currents. The orientation of the instantaneous shear stress under such combined flows reflects mainly the orientation of the wave-induced shear stress. In our opinion, it is the large-scale, high-angle cross-strata that reflect the time-averaged flow direction of the outer boundary layer of a geostrophic current.

Longshore Currents and Net Sediment Drift Were to the South

The modeling suggests that onshore waves along the western shoreline were generated by winds from the north and northeast during the late stages of a winter storm. Argument by analogy with the United States Atlantic coast suggests that these waves would induce a net longshore drift to the south. The four reports of longshore drift in Table 5 (nos. 5, 9, 11, 20) support this idea. In addition, subsurface data of incised, low-stand, conglomeratic shoreline sequences within the Cardium Formation also show a grain-size decrease and inferred longshore-drift direction to the south (unpub. data of A. G. Plint, as reported by W. L. Duke, 1989, personal commun.).

CONCLUSIONS

Numerical simulation of circulation in the Cretaceous Interior Seaway of North America, and comparison of the results with geological observations, suggest that the seaway was largely storm dominated. Wind-driven circulation in the seaway consisted of coast-constrained currents and geostrophic currents flowing parallel to the shoreline and bathymetric contours. Typical winter storms crossing the seaway generated shore-parallel shelf currents of about 0.3 m s^{-1}, first to the north, but ultimately to the south along both shelves, and deep-water waves 4.9 to 5.5 m high with periods on the order of 10 s propagated from the north onto the northwestern shoreline. The resulting prevailing longshore currents and net sediment drift direction were to the south. A more intense storm could have generated shore-parallel currents as strong as 0.8 m s^{-1} along the shelves and 0.4 m s^{-1} in 50 to 100 m of water, and waves 9 m high with periods of 14 s. Tides along the western shores were important mainly in environments conducive to tidal convergence and resonance.

The numerical simulations also indicate that co-oscillating tides propagated into the seaway as progressive Kelvin waves. Meso- to macrotidal ranges are predicted for the southeastern margin, and microtidal ranges are predicted for the remainder of the seaway. We found no published evidence for tides along the southeastern coast, possibly because the evidence is not yet available or was not preserved, or because the margin was significantly shallower than the 25 m used in the modeling.

ACKNOWLEDGMENTS

This work was completed in partial fulfillment of the requirements for the M.S. degree of Marc Ericksen. We thank E. J. Barron and W. L. Duke for assistance and critical reviews of the manuscript. We acknowledge Jim Sloan for providing the CCM data necessary for the study, and Bill Peterson for extensive assistance in developing the graphics programs. Tom Glancy, Don Swift, Dale Leckie, and Dag Nummedal offered thoughtful suggestions. This research was supported by the Société Nationale Elf Aquitaine and The Earth System Science Center and Department of Geosciences at The Pennsylvania State University. It was conducted using the Cornell National Supercomputer Facility, a resource of the Center for Theory and Simulation in Science and Engineering (Cornell Theory Center), which receives major funding from the National Science Foundation and IBM Corporation, with additional support from New York State and members of the Corporate Research Institute.

REFERENCES CITED

Apel, J. R., 1987, Principles of ocean physics: New York, Academic Press, 634 p.

Asquith, D. O., 1970, Depositional topography and major marine environments, Late Cretaceous, Wyoming: American Association of Petroleum Geologists Bulletin, v. 54, p. 1184–1224.

Barron, E. J., 1985, Numerical climate modeling, a frontier in petroleum source rock prediction: Results based on Cretaceous simulations: American Association of Petroleum Geologists Bulletin, v. 69, p. 448–459.

——1989, Severe storms in earth history: Geological Society of America Bulletin, v. 101, p. 601–612.

Barron, E. J., and Washington, W. M., 1982, Cretaceous climate: A comparison of atmospheric simulations with the geologic record: Palaeogeography, Palaeoclimatology, Palaeoecology, v. 40, p. 103–133.

——1984, The role of geographic variables in explaining paleoclimates: Results from Cretaceous climate model sensitivity studies: Journal of Geophysical Research, v. 89, no. D1, p. 1267–1279.

Barron, E. J., Arthur, M. A., and Kauffman, E. G., 1985, Cretaceous rhythmic bedding sequences: A plausible link between orbital variations and climate: Earth and Planetary Science Letters, v. 72, p. 327–340.

Berg, R. R., 1975, Depositional environment of Upper Cretaceous Sussex Sandstone, House Creek field, Wyoming: American Association of Petroleum Geologists Bulletin, v. 59, p. 2099–2110.

Boyles, J. M., and Scott, A. J., 1982a, Comparison of wave-dominated deltaic deposits and associated sand-rich strand plains, Mesaverde Group, north-west Colorado [abs.]: American Association of Petroleum Geologists Bulletin, v. 66, p. 551–552.

——— 1982b, A model for migrating shelf-bar sandstones in Upper Mancos Shale (Campanian), northwestern Colorado: American Association of Petroleum Geologists Bulletin, v. 66, p. 491–508.

Butman, B., Noble, M., and Folger, D. W., 1979, Long-term observations of bottom current and bottom sediment movement on the mid-Atlantic continental shelf: Journal of Geophysical Research, v. 84, no. C3, p. 1187–1205.

Campbell, C. V., 1971, Depositional model—Upper Cretaceous Gallup beach shoreline, Ship Rock area, northwestern New Mexico: Journal of Sedimentary Petrology, v. 41, p. 395–409.

Campbell, C. V., and Oaks, R. Q., 1973, Estuarine sandstone filling tidal scours, Lower Cretaceous Fall River Formation, Wyoming: Journal of Sedimentary Petrology, v. 43, p. 765–778.

Carmicheal, S.S.M., 1988, Linear estuarine conglomerate bodies formed during a mid-Albian marine transgression; "Upper Gates" Formation, Rocky Mountain foothills of northeastern British Columbia, in James, D. P., and Leckie, D. A., eds., Sequences, stratigraphy, sedimentology: Surface and subsurface: Canadian Society of Petroleum Geologists Memoir 15, p. 49–62.

Coachman, L. K., and Aagaard, K., 1974, Physical oceanography of Arctic and subarctic seas, in Herman, Y., ed., Marine geology and oceanography of the Arctic seas: New York, Springer-Verlag, 397 p.

Cotter, E., 1975, Late Cretaceous sedimentation in a low-energy coastal zone: The Ferron Sandstone of Utah: Journal of Sedimentary Petrology, v. 45, p. 669–685.

Csanady, G. T., 1982, Circulation in the coastal ocean: Boston, Massachusetts, D. Reidel Publishing Company, 311 p.

Davis, H. R., and Byers, C. W., 1989, Shelf sandstones in the Mowry Shale: Evidence for deposition during Cretaceous sea level falls: Journal of Sedimentary Petrology, v. 59, p. 546–560.

Defant, A., 1958, Ebb and flow, the tides of earth, air, and water: Ann Arbor, Michigan, The University of Michigan Press, 121 p.

Duke, W. L., 1981, Internal stratigraphy and paleogeography of the Upper Cretaceous Cardium Formation in the Alberta foothills [abs.]: Geological Association of Canada Abstracts 6, p. A–38.

——— 1985, Hummocky cross-stratification, tropical hurricanes, and intense winter storms: Sedimentology, p. 167–194.

——— in press, Geostrophic circulation or shallow marine turbidity currents? The dilemma of paleoflow patterns in storm-influenced prograding shoreline systems: Journal of Sedimentary Petrology.

Duke, W. L., Ainsworth, B. H., and Walker, R. G., 1980, Storm-dominated coarsening-upward clastic sequences in the Cardium, Upper Cretaceous, southern Alberta [abs.]: Geological Society of America Abstracts with Programs, v. 12, p. 32.

Eicher, D. L., 1969, Paleobathymetry of Cretaceous Greenhorn Sea in eastern Colorado: American Association of Petroleum Geologists Bulletin, v. 53, p. 1075–1090.

——— 1987, Paleobathymetry in the Cretaceous Western Interior Seaway [abs.]: Society of Economic Paleontologists and Mineralogists, 1987 Midyear Meeting.

Ericksen, M., Masson, D., Slingerland, R., and Swetland, D., 1989, Numerical simulation of circulation and sediment transport in the Late Devonian Catskill Sea, in Cross, T. A., ed., Quantitative dynamic stratigraphy: Englewood Cliffs, New Jersey, Prentice-Hall, p. 293–305.

Evans, W. E., 1966, Imbricate linear sandstone bodies of Viking Formation in Dodsland-Hoosier area of southwestern Saskatchewan, Canada: American Association of Petroleum Geologists Bulletin, v. 54, p. 469–486.

Gaynor, G. C., and Swift, D.J.P., 1988, Shannon Sandstone depositional model: Sand ridge dynamics on the Campanian western interior shelf: Journal of Sedimentary Petrology, v. 58, p. 868–880.

Gill, A. E., 1982, Atmospheric-ocean dynamics: New York, Academic Press, 662 p.

Harms, J. C., Southard, J. B., and Walker, R. G., 1982, Structures and sequences in clastic rocks: Society of Economic Paleontologists and Mineralogists Short Course No. 9.

Heaps, N. S., ed., 1987, Three-dimensional coastal ocean models: Washington, D.C., American Geophysical Union Coastal and Estuarine Sciences 4, 208 p.

Hobday, D. K., and Morton, R. A., 1984, Lower Cretaceous shelf storm deposits, northeast Texas, in Tillman, R. W., and Siemers, C. T., Siliciclastic shelf sediments: Society of Economic Paleontologists and Mineralogists Special Publication No. 34, p. 205–213.

Howard, J. D., Kamola, D., and Salazar, A., 1982, Depositional facies of Cretaceous Spring Canyon Member, Blackhawk Formation, Book Cliffs, Utah [abs.]: American Association of Petroleum Geologists Bulletin, v. 66, p. 584.

Kamola, D., and Howard, J. D., 1983, Barrier island, tidal inlet, and flood tidal delta deposits of the Upper Cretaceous Spring Canyon Mbr., Blackhawk Fm. [abs.], in Stott, D. F., and Glass, D. J., eds., The Mesozoic of middle North America: Canadian Society of Petroleum Geologists Memoir 9, p. 569.

Kauffman, E. G., 1977, Geological and biological overview: Western Interior Cretaceous basin: The Mountain Geologist, v. 14, p. 75–99.

——— 1984, Paleobiogeography and evolutionary response dynamics in the Cretaceous Western Interior Seaway of North America, in Westermann, G.E.G., ed., Jurassic-Cretaceous biochronology and paleogeography of North America: Geological Association of Canada Special Paper 27, p. 273–306.

——— 1985, Cretaceous evolution of the Western Interior Basin of the United States, in Pratt, L. M., Kauffman, E. G., and Zelt, F. B., eds., Fine-grained deposits and biofacies of the Cretaceous Western Interior Seaway: Evidence of cyclic sedimentary processes: Society of Economic Paleontologists and Mineralogists, 1985 Midyear Meeting, Golden, Colorado, Field Trip Guidebook No. 4.

Kiteley, L., and Field, M., 1984, Shallow marine depositional environments in the Upper Cretaceous of northern Colorado, in Siliciclastic shelf sediments: Society of Economic Paleontologists and Mineralogists Special Publication No. 34, p. 179–204.

Klein, G. D., and Ryer, T. A., 1978, Tidal circulation patterns in Precambrian, Paleozoic, and Cretaceous epeiric and mioclinal shelf seas: Geological Society of America Bulletin, v. 89, p. 1050–1058.

Komar, P. D., 1976, Beach processes and sedimentation: Englewood Cliffs, New Jersey, Prentice-Hall, Inc., 429 p.

Koutitas, C. G., 1988, Mathematical models in coastal engineering: London, England, Pentech Press, 156 p.

Leckie, D., 1986, Tidally influenced, transgressive shelf sediments in the Viking Formation, Caroline, Alberta: Bulletin of Canadian Petroleum Geology, v. 34, p. 111–125.

Leckie, D. A., and Krystinik, L. F., 1989, Is there evidence for geostrophic currents preserved in the sedimentary record of inner- to middle-shelf deposits?: Journal of Sedimentary Petrology, v. 59, p. 862–870.

Leckie, D. A., and Walker, R. G., 1982, Storm- and tide-dominated shorelines in Cretaceous Moosebar–Lower Gates interval—Outcrop equivalents of deep basin gas trap in western Canada: American Association of Petroleum Geologists Bulletin, v. 66, p. 138–157.

Leckie, D. A., Cheel, R. J., and Rosenthal, L., 1989, Sedimentology of the Upper Virgelle Member (Upper Cretaceous Milk River Formation), Writing-on-Stone Provincial Park, Alberta and the Southern Alberta Transect: Canadian Society of Petroleum Geologists, Second International Research Symposium on Clastic Tidal Deposits, Calgary, Alberta, 49 p.

Lee, T. N., Kourafalou, V., Wang, J. D., Ho, W. J., Blanton, J. O., Atkinson, L. P., and Pietrafesa, L. J., 1985, Shelf circulation from Cape Canaveral to Cape Fear during winter, in Atkinson, L. P., Menzel, D. W., and Bush, K. A., eds., Oceanography of the southeastern U.S. continental shelf: American Geophysical Union, 1985, p. 33–76.

Leendertse, J. J., and Liu, S., 1975, A three-dimensional model for estuaries and coastal seas: Volume II, Aspects of computation: Rand R-1764-OWRT, 123 p.

——— 1977, A three-dimensional model for estuaries and coastal seas: Volume IV, Turbulent energy computation: Rand R-2187-OWRT, 59 p.

——— 1979, A three-dimensional model for estuaries and coastal seas: Volume VI, Bristol Bay simulations: Rand R-2405-NOAA, 121 p.

Leendertse, J. J., Alexander, R. C., and Liu, S., 1973, A three-dimensional model for estuaries and coastal seas: Volume I, Principles of computation: Rand R-1417-OWRR, 57 p.

Liu, S., and Nelson, A. B., 1977, A three-dimensional model for estuaries and coastal seas: Volume V, Turbulent energy program: Rand R-2188-OWRT, 90 p.

Lloyd, C. R., 1982, The mid-Cretaceous earth: Paleogeography; ocean circulation and temperature; atmospheric circulation: Journal of Geology, v. 90, p. 393–413.

Lorsong, J. A., 1982, Channels and chimeras: Coastal vs. fluvial deposition of Manneville Group, Lloydminster area, Saskatchewan [abs.]: American Association of Petroleum Geologists Bulletin, v. 66, p. 596.

MacKenzie, D. B., 1972, Tidal and sand flat deposits in Lower Cretaceous Dakota Group near Denver, Colorado: Mountain Geologist, v. 9, p. 269–277.

Masters, C. D., 1967, Use of sedimentary structures in determination of depositional environment, Mesaverde Formation, Williams Fork Mountain, Colorado: American Association of Petroleum Geologists Bulletin, v. 51, p. 2033–2043.

Meijer Drees, N. C., and Myhr, D. W., 1981, The Upper Cretaceous Milk River and Lea Park Formations in southeastern Alberta: Bulletin of Canadian Petroleum Geologists, v. 29, p. 42–71.

Niedoroda, A. W., and Swift, D.J.P., Hopkins, T. S., and Ma, C. M., 1984, Shoreface morphodynamics on wave-dominated coasts, in Greenwood, B., and others, eds., Hydrodynamics and sedimentation in wave-dominated coastal environments: Marine Geology, v. 60, p. 331–354.

Nihoul, J.C.J., 1982, Hydrodynamic models of shallow continental seas; Application to the North Sea: Neupre, Etiene RIGA, editeur, 198 p.

Nummedal, Dag, and Swift, D.J.P., 1987, Transgressive stratigraphy at sequence-bounding unconformities; some principles derived from Holocene and Cretaceous examples, in Nummedal, Dag, and others, eds., Sea-level fluctuations and coastal evolution: Society of Economic Paleontologists and Mineralogists Special Publication 41, p. 241–260.

Parrish, J. T., and Curtis, R. L., 1982, Atmospheric circulation, upwelling and organic-rich rocks in the Mesozoic and Cenozoic Eras: Palaeogeography, Palaeoclimatology, Palaeoecology, v. 40, p. 31–66.

Parrish, J. T., Gaynor, G. C., and Swift, D.J.P., 1984, Circulation in the Cretaceous Western Interior Seaway of North America, a review, in Stott, D. F., and Glass, D. J., eds., The Mesozoic of middle North America: Canadian Society of Petroleum Geologists Memoir 9, p. 221–231.

Pond, S., and Pickard, G. L., 1983, Introductory dynamical oceanography: New York, Pergamon Press, 329 p.

Rahmani, R. A., 1988, Estuarine tidal channel and nearshore sedimentation of a Late Cretaceous epicontinental sea, Drumheller, Alberta, Canada, in de Boer and others, eds., Tide-influenced sedimentary environments and facies: Boston, Massachusetts, D. Reidel Publishing Company, p. 433–471.

Rahmani, R. A., and Smith, D. G., 1988, The Cadotte Member of northwestern Alberta: A high-energy barred shoreline, in James, D. P., and Leckie, D. A., eds., Sequences, stratigraphy, sedimentology: Surface and subsurface: Canadian Society of Petroleum Geologists Memoir 15, p. 431–438.

Redfield, A. C., 1980, Introduction to tides, the tides of the waters of New England and New York: Woods Hole, Massachusetts, Marine Science International, 108 p.

Reinson, G. E., Clark, J. E., and Foscolos, A. E., 1988, Reservoir geology of Crystal Viking field, Lower Cretaceous estuarine tidal channel-bay complex, south-central Alberta: American Association of Petroleum Geologists Bulletin, v. 72, p. 1270–1294.

Rice, D. D., 1980, Coastal and deltaic sedimentation of Upper Cretaceous Eagle Sandstone: Relation to shallow gas accumulations, north-central Montana: American Association of Petroleum Geologists Bulletin, v. 64, p. 316–338.

——— 1984, Widespread, shallow marine, storm-generated sandstone units in the Upper Cretaceous Mosby Sandstone, central Montana, in Siliciclastic shelf sediments: Society of Economic Paleontologists and Mineralogists Special Publication No. 34, p. 143–162.

Ryer, T. A., and Kauffman, E. G., 1980, Physical evidence for Cretaceous tides, Western Interior Basin, North America [abs.]: American Association of Petroleum Geologists Bulletin, v. 64, p. 778.

Shurr, G. W., 1984, Regional setting of Niobrara Formation in northern Great Plains: American Association of Petroleum Geologists Bulletin, v. 68, p. 598–609.

Slater, R. D., 1985, A numerical model of tides in the Cretaceous Seaway of North America: Journal of Geology, v. 93, p. 333–345.

Slingerland, R., 1977, Processes, responses, and resulting stratigraphic sequences of barrier island tidal inlets as deduced from Assawoman inlet, Va. [Ph.D. thesis]: University Park, Pennsylvania, Pennsylvania State University, 387 p.

——— 1986, Numerical computation of co-oscillating palaeotides in the Catskill epeiric sea of eastern North America: Sedimentology, v. 33, p. 487–497.

Spearing, D. R., 1976, Upper Cretaceous Shannon Sandstone: An offshore, shallow-marine sand body: Wyoming Geological Association, 28th Annual Field Conference, Guidebook, p. 65–72.

Swift, D.J.P., and Niedoroda, A. W., 1985, Fluid and sediment dynamics on continental shelves, in Tillman, R. W., Swift, D.J.P., and Walker, R. G., eds., Shelf sands and sandstone reservoirs: Society of Economic Paleontologists and Mineralogists Short Course Notes No. 13, p. 47–133.

Swift, D. J., and Rice, D. D., 1984, Sand bodies on muddy shelves: A model for sedimentation in the Western Interior Seaway, North America, in Tillman, R. W., and Siemers, C. T., Siliciclastic shelf sediments: Society of Economic Paleontologists and Mineralogists Special Publication No. 34, p. 43–62.

Swift, D.J.P., Han, G., and Vincent, C. E., 1986a, Fluid processes and sea-floor response on a modern storm-dominated shelf: Middle Atlantic shelf of North America. Part I: The storm-current regime, in Knight, R. J., and McLean, J. R., eds., Shelf sands and sandstones: Canadian Society of Petroleum Geologists Memoir II, p. 99–119.

Swift, D.J.P., Thorne, J. A., and Oertal, G. A., 1986b, Fluid processes and sea-floor response on a modern storm-dominated shelf: Middle Atlantic shelf of North America. Part II: Response of the shelf floor, in Knight, R. J., and McLean, J. R., eds., Shelf sands and sandstones: Canadian Society of Petroleum Geologists Memoir II, p. 191–211.

Swift, D.J.P., Hudelson, P. M., Brenner, R. L., and Thompson, P., 1987, Shelf construction in a foreland basin: Storm beds, shelf sandbodies, and shelf-slope depositional sequences in the Upper Cretaceous Mesaverde Group, Book Cliffs, Utah: Sedimentology, v. 34, p. 423–457.

Thorne, J. A., and Swift, D.J.P., 1985, A theory of tidal amplification in coastal embayments and open shelves: Application to ancient marine sedimentation [abs.]: Symposium on modern and ancient clastic tidal deposits, Utrecht, The Netherlands, University of Utrecht, 26–28 August, p. 141–144.

Tillman, R. W., and Martinsen, R. S., 1984, The Shannon shelf-ridge sandstone complex, Salt Creek anticline area, Powder River Basin, Wyoming, in Tillman, R. W., and Siemers, C. T., eds., Siliciclastic shelf sediments: Society of Economic Paleontologists and Mineralogists Special Publication No. 34, p. 85–142.

U.S. Army Coastal Engineering Research Center (CERC), 1975, Shore protection manual.

Vincent, C. E., 1986, Processes affecting sand transport on a storm-dominated shelf, in Knight, R. J., and McLean, J. R., eds., Shelf sands and sandstones: Canadian Society of Petroleum Geologists Memoir II, p. 191–211.

Wallace-Dudley, K. E., and Leckie, D. A., 1988, Preliminary observations on the sedimentology of the Doe Creek Member, Kaskapau Formation, in the Valhalla Field, northwestern Alberta, in James, D. P., and Leckie, D. A., eds., Sequences, stratigraphy, sedimentology: Surface and subsurface: Canadian Society of Petroleum Geologists Memoir 15, p. 485–496.

Weimer, R. J., 1966, Time stratigraphic analysis and petroleum accumulations, Patrick Draw Field, Sweetwater County, Wyoming: American Association of Petroleum Geologists Bulletin, v. 50, p. 2150–2175.

Williams, G. D., and Stelk, C. R., 1975, Speculations of the Cretaceous palaeogeography of North America, in Caldwell, W.G.E., ed., The Cretaceous system in the Western Interior of North America: Geological Association of Canada Special Paper No. 13, p. 1–20.

Winker, C. D., and Buffler, R. T., 1988, Paleogeographic evolution of early deep-water Gulf of Mexico and margins, Jurassic to Middle Cretaceous (Comanchean): American Association of Petroleum Geologists Bulletin, v. 72, p. 318–346.

Winn, R. D., Jr., Stonecipher, S. A., and Bishop, M. G., 1983, Depositional environments and diagenesis of offshore sand ridges, Frontier Formation, Spearhead Ranch Field, Wyoming: Mountain Geologist, v. 20, p. 41–58.

Winn, R. D., Jr., Bishop, M. G., and Gardner, P. S., 1987, Shallow-water and sub-storm-base deposition of Lewis Shale in Cretaceous Western Interior Seaway, south-central Wyoming: American Association of Petroleum Geologists Bulletin, v. 71, p. 859–881.

Wright, E. K., 1987, Stratification and paleocirculation of the Late Cretaceous Western Interior Seaway of North America: Geological Society of America Bulletin, v. 99, p. 480–490.

Manuscript Received by the Society April 7, 1989
Revised Manuscript Received February 21, 1990
Manuscript Accepted February 28, 1990